Expertise
and insight
for the future

Yuliia Korniushyna

# The Reliability Study of Red Phosphorus Containing Insulation of a DC plug

Metropolia University of Applied Sciences

Bachelor of Engineering

Degree Programme in Electronics

Bachelor's Thesis

14 May 2020

| | |
|---|---|
| Author<br>Title<br><br>Number of Pages<br>Date | Yuliia Korniushyna<br>The Reliability Study of Red Phosphorus Containing Insulation of a DC plug<br>48 pages + 4 appendices<br>14 May 2020 |
| Degree | Bachelor of Engineering |
| Degree Programme | Degree Programme in Electronics |
| Professional Major | Electronics |
| Instructors | Heikki Valmu, Supervisor, Principal Lecturer<br>Esko Honkala, Instructor, Electrical Engineer at KaVo Kerr |

This Bachelor's Thesis is a report on the preparation for and practical implementation of the reliability study of red phosphorus containing DC plug's insulation. KaVo Kerr had received some seven-year-old DC plugs containing red phosphorus as a flame retardant, according to the manufacturer, and the reliability of DC plug's insulation had to be assessed due to red phosphorus reliability issues known in electronics industry.

Red phosphorus failure behaviour includes formation of conductive paths in the insulation under elevated temperature and humidity conditions and voltage bias, therefore DC plugs were subjected to the temperature-humidity-bias test, throughout which the leakage current flowing through the insulation was being measured. The setup for current measurement of 50uA – 100mA range was designed, built and verified over the course of the work in preparation for the study.

Results of the study indicate that red phosphorus containing insulation of a DC plug developed leakage current up to 100mA under 80ºC/80%RH/24V conditions in under 13 hours. Leakage current showed intermittent character and the traces of corrosion were observed on some of the plugs after the test.

Used red phosphorus manufacturing process is unknown, therefore results are of limited value. Experiment outcomes nevertheless encourage careful consideration and testing of red phosphorus containing materials prior to their long-term use in electronics applications.

Further study of the physical and chemical processes that led to the leakage current formation in DC plugs' insulation is recommended.

| | |
|---|---|
| Keywords | red phosphorus, insulation failure, electronics reliability |

## Contents

## List of Abbreviations

| | |
|---|---|
| ADC | Analog-to-Digital Converter. A system that transforms analog signal into digital form following, for example, a successive approximation procedure. |
| CMRR | Common-mode rejection ratio. A parameter of, for example, an operational amplifier qualifying the ability of the amplifier to reject the common-mode voltage, that is, the voltage present on the both inputs simultaneously. |
| PCB | Printed-circuit board. A board supporting electronics components physically and providing connection paths for electronics components. |
| PCBA | Printed-circuit board assembly. A PCB with components assembled. |
| RH | Relative Humidity. The ratio of the partial pressure of water vapor to the equilibrium vapor pressure of water at a given temperature. |
| RP | Red phosphorus. A chemical, an allotrope of white phosphorus, which is also used as a flame retardant. |
| THB | Temperature-humidity-bias test. Standard accelerated lifetime test, where object under test is subjected to high temperature, humidity and voltage bias. |

# 1 Introduction

KaVo Kerr, as Dental Imagining devices manufacturer, had been provided with some samples of third-party DC plugs for use with power supplies of over seven-years-old medical devices, claimed to contain red phosphorus as a flame retardant by the manufacturer. Having heard from customers about general reliability issues in electronics components induced by red phosphorus, KaVo Kerr expressed the need for the thorough investigation of provided for the evaluation DC plugs. Samples were studied in a third-party laboratory and were concluded to contain phosphorus. However, the studies did not provide specific information on the elemental phosphorus content in a red phosphorus allotrope form and the possible red phosphorus manufacturing process used. Therefore, KaVo Kerr decided to conduct an internal investigation on the reliability of provided samples.

The goal of this the work was thus to conduct the reliability study of provided DC plug samples considering the potential failure behavior of red phosphorus containing insulation presented in the literature.

It has to be stated that the behavior of red phosphorus in electronics components largely depend on the manufacturing process and compounds used, as will be later described in the literature review. The manufacturing process and the detailed compound of the DC plug insulation material are unknown, and therefore this work cannot possibly draw any conclusions neither on the properties of the material nor on the manufacturing process used.

# 2 Theoretical Background

## 2.1 Flame Retardants and the Mechanism of Flame Suppression

Flame retardants are chemicals introduced into encapsulates and molding compounds to improve the ability of a material to withstand ignition and combustion.

Flame retardants include a variety of chemicals: halogenated compounds, phosphorus compounds, inorganic compounds, nitrogen-containing organic compounds, silicone compounds, etc., which differ in relation to the way they are introduced to the material – either chemically or mechanically, and in relation to the way they operate. [1.]

Flame retardants are divided into two groups based on their flame retardancy mechanism. Flame retardants operating in a so-called vapor phase, such as halogen compounds, phosphorus compounds and hydrated metal compounds, are activated in the initial combustion phase of a material, when a polymer is being decomposed under heat and combustible gas is being generated, igniting and accelerating the temperature rise further (see figure 1) [1,7].

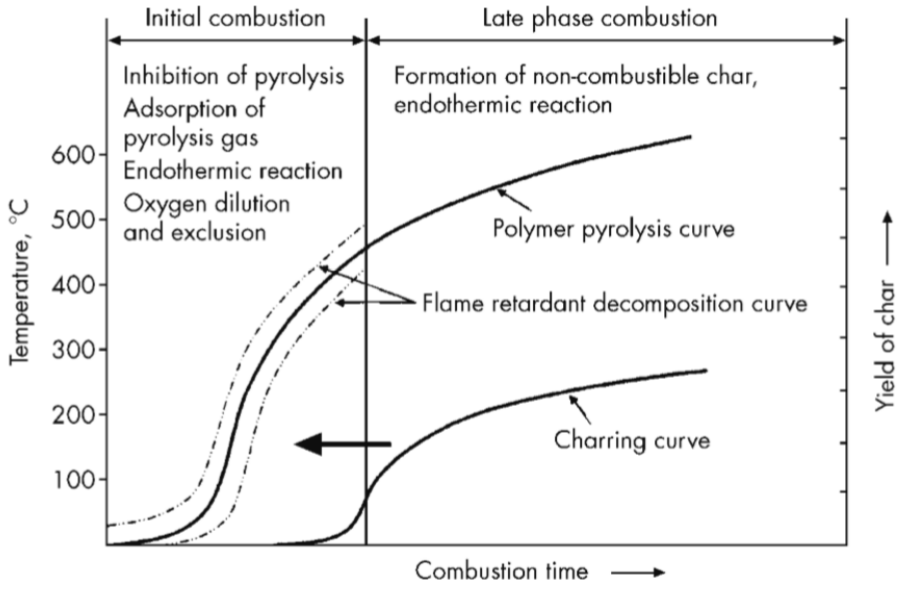


Figure 1. Phases of combustion. Copied from Nishizawa [1,8].

The main objectives for flame retardants operating in a vapor phase are to provide a free-radical trapping effect, which would prevent combustible gas generation, to dilute oxygen with incombustible gas or to prevent oxygen from reacting with a material altogether and to initiate an endothermic reaction which would prevent the temperature rise (see figure 2) [1,7].

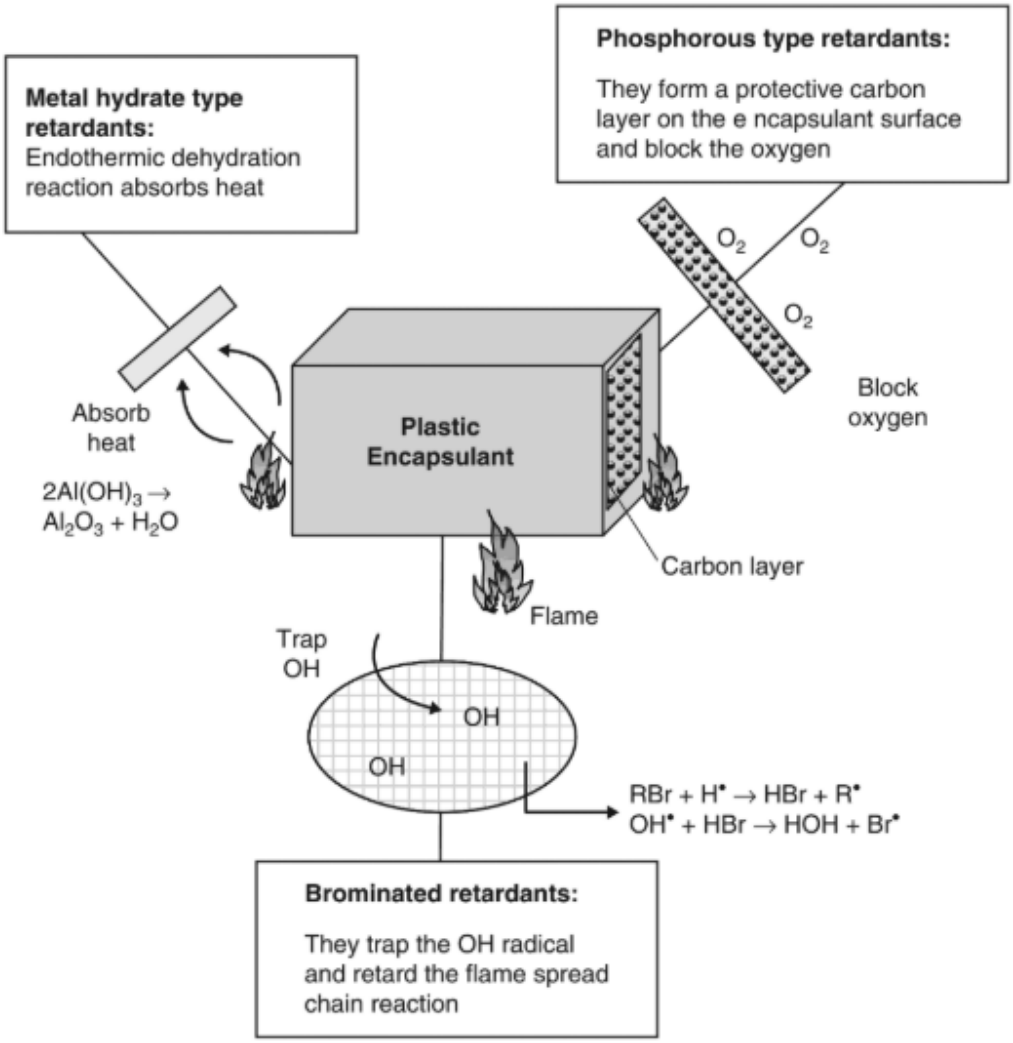


Figure 2. Operation of flame retardants in a vapor phase. Copied from Ardebili and Pecht [2,112].

Another group of flame retardants operates at a late combustion state, when the char formation progresses (see figure 1). The main objectives of this group of retardants are to facilitate the formation of graphitic char as a combustion residue or to exclude oxygen supply to a polymer surface by an inorganic oxide layer creation. [1,7.]

## 2.2 Red Phosphorus as a Flame Retardant

Red phosphorus flame retardants belong to the phosphorus group of retardants, which facilitate char creation and block the oxygen supply to the burning material. The development of red phosphorus flame retardants, which are claimed to be environmentally friendly compounds, has been motivated by the partial ban on brominated retardants with RoHS directives due to their harmful environmental implications [3,54].

However, red phosphorus flame retardants are also known in the industry for affecting the range of product recalls and reliability alerts, including products of such companies as Maxim Integrated Products, Fujitsu, Hitachi, Fairchild Semiconductor, Motorola, etc. [4,805], which was a primary reason for its being under investigation in this work.

Red phosphorus is an allotropic form of elemental phosphorus and is manufactured by heating white phosphorus with 250 – 300ºC or exposing it to light in order to re-arrange the structure of the chemical (see figure 3), and then grinding [5,7-9], and the end product is claimed to be a non-toxic, insoluble in solvents material [6,817].

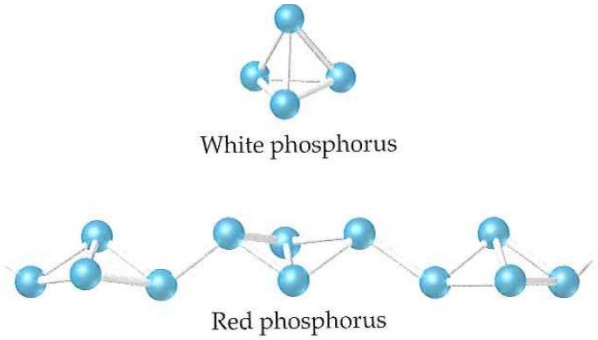


Figure 3. Red phosphorus vs. white phosphorus structure. Copied from Wilson [7].

However, in the process of various scientific research [6;8], red phosphorus was found to be sensitive to moist air, forming $PO_4^{3-}$ ions and releasing various phosphorus-containing acids, oxides and phosphine gas $PH_3$, as described by the equations presented on figure 4:

$$4P + 5O_2 \longrightarrow 2P_2O_5 \uparrow$$
$$P_2O_5 + 3H_2O \longrightarrow 2H_3PO_4 \uparrow$$
$$4P + 6H_2O \longrightarrow 2H_3PO_3 + 2PH_3 \uparrow$$
$$4H_3PO_3 \longrightarrow 3H_3PO_4 + PH_3 \uparrow$$

Figure 4. Red phosphorus reactions in moist air. Copied from Somayajulu *et al.* [6, 818].

Phosphoric acid ($H_3PO_4$) is corrosive and can act as an electrolyte, thus causing an electrochemical migration, that is, the dissolution and movement of metal ions under an electrical potential, which leads to formations of conductive paths (for example, dendrites) in-between leads of an opposite potential [5,13], as shown on figure 5:

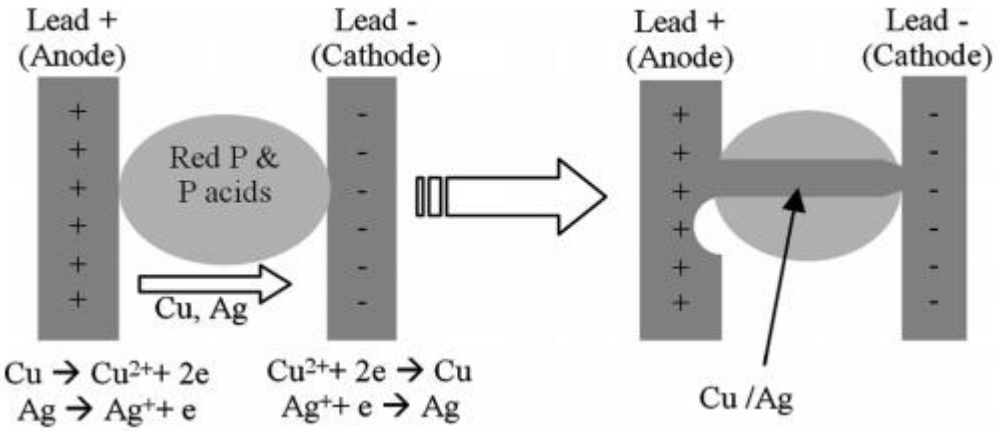


Figure 5. An electrochemical migration in the acid environment. Copied from Deng *et al.* [4,807].

As the process continues and the formation of acid accelerates, degradation of a mold compound accelerates and leakage current increases, eventually leading to the failure event. [8,24937.]

Below is the example presented in the investigation conducted on the failed IC chip (see figure 6):

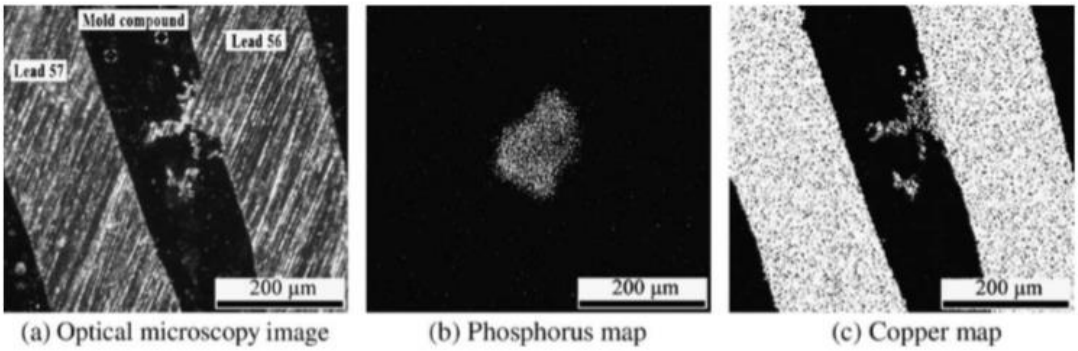


Figure 6. Examples of a short circuit path formation between adjacent leads of the IC chip. Copied from Pecht and Deng [3,59].

It is also particularly interesting that the failure behavior may be intermittent, according to Wang *et al.* [9] research paper stating that:

> The acid also etched copper as a chemical reaction. It explained why the failure is intermittent and flickered: the sample can be occasionally recovered for short time if the acid etches the fine copper away and disconnects the shorting path. [9,581.]

The conductive path can also be fused if too high current flows through it and burns the dendrite, making this failure behavior particularly challenging to test for in the manufacturing and testing process of the IC chips, as Hylton [10,113] paper discusses. Hylton [10] also points out that the failure has an intermittent character:

> Instability in the leakage will often be observed, with the measured resistance quickly fluctuating, even intermittently appearing as an open circuit. [10,113.]

To improve the reliability of red phosphorus containing materials, manufacturers have introduced a range of process changes, such as decreasing the size of red phosphorus particles to around 50um (such that they are not bridging adjacent leads of integrated circuits), changing the red phosphorus manufacturing process such that particles acquire a spherical form (to further reduce susceptibility to moisture and oxidation) and double-coating of RP particles: first, with some metal dioxide (so-called stabilizer) to stabilize an acid formation and second, with some thermosetting resin (for example, phenolic resin) to increase the resistance against heat degradation. [5.]

Double-coating of red phosphorus particles had initially been believed to be a sufficient countermeasure for heat and moisture sensitivity of red phosphorus particles, yet in 2000

manufacturers admitted, that even this solution is not sufficient for components requiring high moisture resistivity:

> However, phosphate ion [$PO_4^{3-}$] and phosphite ion [$PO_3^{3-}$] eluting from this [double-coated red phosphorus] flame retardant adversely affect moldability and curability of the resin composition and moisture resistance and electric characteristics of the resulting semiconductors. . . . [5,12.]

Failure of the double-coating process has been believed to be the root cause of the whole chain event: either the quality of the double-coating process has been initially deficient, or the double-coating of red phosphorus particles has deteriorated as a consequence of a thermal treatment [11,3]. For example, Deng and Pecht [11,3] paper suggests that typically used aluminum hydroxide $Al(OH)_3$ coating can decompose to alumina and water as a result of a 190 – 250ºC temperature treatment according to the following formula:

$$2Al(OH)_3 \rightarrow 3H_2O + Al_2O_3. \quad (1)$$

With the aluminum hydroxide decomposition and the following water formation, the moisture content of the mold compound increases, which under the oxygen influence facilitates the phosphoric ions $PO_x$ and phosphorus-based acids formation [11,3], which in turn initiates the chain of events.

It is also pointed out in the Deng and Pecht [11] paper that “the typical temperature for the transfer molding process is around 175°C, and temperatures for reflow soldering are around 220°C” [11,3], meaning that the coating decomposition might be initiated by standard manufacturing processes.

The studies focused on the red phosphorus containing materials’ properties investigation provide a variety of results on analysing moisture content, acid content, and phosphine content changes over time under various environmental conditions. Hillman [12], for example, presents the dependency of the moisture content of the red phosphorus containing material in relation to temperature, humidity and time, indicating that moisture is absorbed faster with increased temperature and humidity (see figure 7):

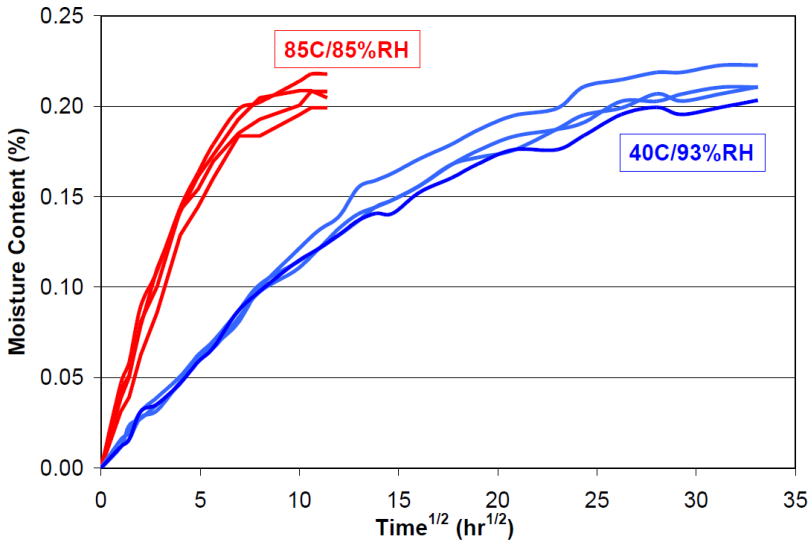


Figure 7. The dependency of red phosphorus containing material's moisture content on temperature, humidity and time. Copied from Hillman [12,18].

Rin Kagaku Kogyo Co., Ltd. also presents on the company's website some graphical information on phosphine emissions and the conductivity of an untreated red phosphorus epoxy resin and several other manufacturer's red phosphorus containing products [13]. The red phosphorus containing materials' phosphine emission dependency on temperature is presented on figure 8, indicating that red phosphorus's reactivity generally increases with temperature and varies in different products:

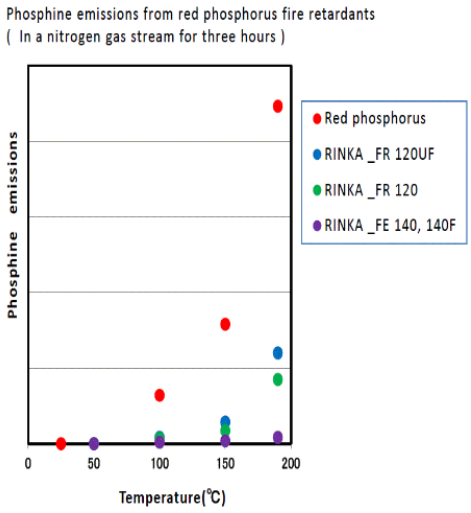


Figure 8. The dependence of phosphine emissions from red phosphorus containing materials on temperature. Copied from Rin Kagaku Kogyo Co., Ltd. webpage [13].

The red phosphorus containing materials' conductivity dependence on time is presented on figure 9, showing an overall increase in conductivity of soaked in water materials with time. Conductivity varies depending on the product as well.

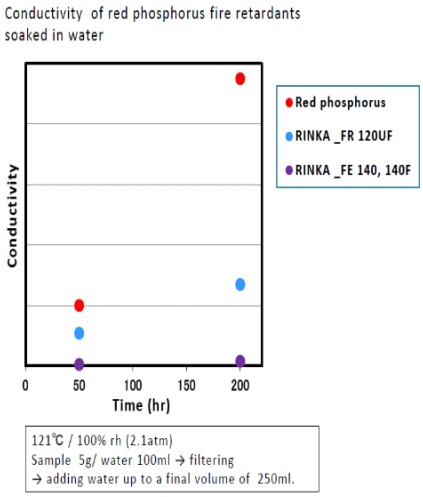


Figure 9. The dependence of red phosphorus containing materials' conductivity on time. Copied from Rin Kagaku Kogyo Co., Ltd. webpage [13].

Results presented in Somayajulu *et al*. [6] research paper indicate that moisture absorbtion of red phosphorus containing materials depends on a stabilizer used in the red phosphorus manufacturing process, see figure 10:

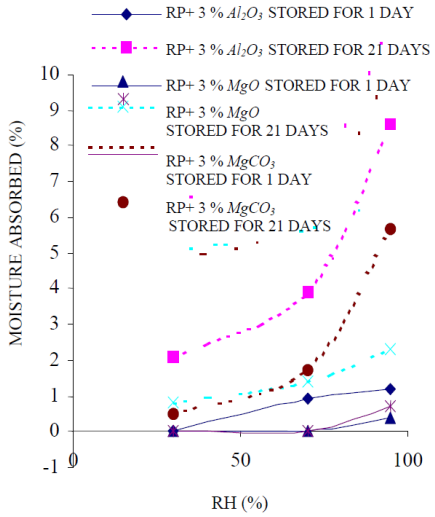


Figure 10. Moisture absorption of red phosphorus with different stabilizers in a room temperature. Copied from Somayajulu *et al.* [6,821].

Somayajulu *et al.* [6] research paper also indicates that phosphine release of red phosphorus containing compositions depends on a stabilizer used in the red phosphorus manufacturing, see figure 11:

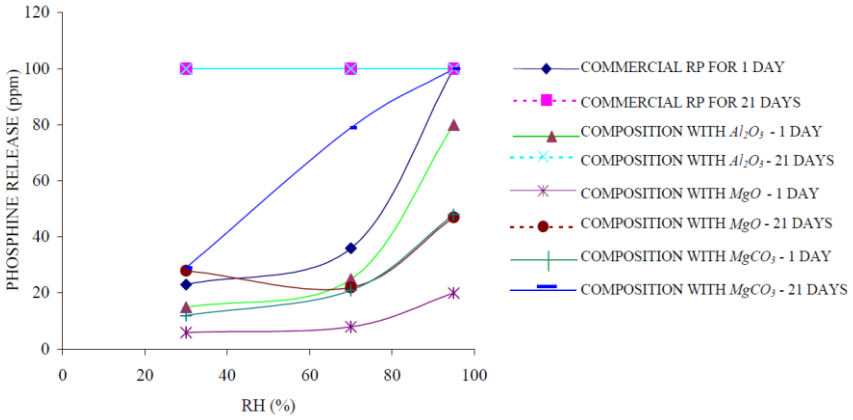


Figure 11. Phosphine release of red phosphorus compositions in a room temperature using different stabilizers. Copied from Somayajulu *et al.* [6,821].

It follows from figures 7-11 presented above that moisture absorption and phosphine formation depend on humidity exponentially regardless of the coating composition, phosphine emissions increase exponentially with temperature, conductivity increases with time, and the rate of moisture content increase depends on humidity and temperature.

It has to be said that the development of red phosphorus manufacturing processes constantly progresses, and scientific evidence presented in this literature review mostly covers manufacturing technology and failure investigation studies of years 2000 – 2010. However, the plugs under investigation are seven years old and might have been manufactured with an improved technology. There is limited scientific evidence of failure investigations conducted during recent years presented in this literature review. Advances in the red phosphorus manufacturing technology were also not investigated, as the manufacturing process of plugs under evaluation is unknown. It is thus theoretically possible that recent advances in the red phosphorus manufacturing have eliminated red phosphorus conductivity issues, and it cannot be stated that generally all red phosphorus containing materials are necessarily dangerous. However, results of the studies presented above suggest that caution shall be exercised when selecting red phosphorus containing materials for product development purposes.

Overall, the literature review indicates that possible chemical processes leading to the failure event in the form of leakage current path formation can be accelerated under higher humidity and higher temperature conditions, and the failure behaviour is expected to be intermittent.

# 3 Practical Experiment

## 3.1 Setup Requirements Overview

The literature review suggested that the insulation failures affected by red phosphorus manifest themselves as conductive path formations. To account for such behavior, the reliability test setup had to incorporate current sensing capability.

Below are general requirements for the test setup that provided an input to the further design thinking:

- The setup had to reliably measure currents flowing through the insulation of the plug in the range of 50uA – 100mA. The rationale for the range had its origins from the Medical Electric Safety standard IEC60601-1 [14]. Even though the standard could not be applied in a given situation, as the rated voltage across plug is relatively low (24V), the standard nevertheless gives limits for Earth Leakage currents (currents flowing through an insulation between the mains wire and the earth conductor [14,25]), being 5mA in the normal condition and 10mA in the single fault condition [14,90], such as when one mains wire is broken [14,72]. Those limits signify that leakage current above 5mA can be surely considered unacceptable. Also, the same standard specifies the value of 15W as a limit for the maximum power generated by the component to be safe from the flammability point of view [14,174]. Therefore, 15W/24V = 0.625A current could potentially constitute the risk of fire. To avoid the risk of fire with a substantial margin and to obtain as detailed information as to the leakage current development as design-wise possible, the range was selected to be 50uA – 100mA.

- The setup had to record the average, maximum and minimum value of the current measured during each second.

- The whole test had to stop after the measured current had reached 100mA value.

- The environmental conditions for the test had to be 80°C/80%RH to facilitate accelerated aging of the insulation. The plug's insulation had to be energized by 24V as in a normal operation. The conditions were derived combining the 85/85 temperature-humidity bias (THB) test specified by industry standards [15,427] and challenges related to practical implementation of the test (unrelated to the current thesis work R&D test had to be conducted in a climatic chamber with conditions 80/80 simultaneously with this test). Standards differ in their requirements as to the recommended duration of the test, however the minimum recommended 168h or one week duration was selected given the project schedule limitations.

The test had to be carried out for two plugs simultaneously: one that assuredly does not contain red phosphorus as a flame retardant in the insulation of the plug, and the allegedly red phosphorus containing plug.

At the end of the test, graphs had to be built for the current changes' dependency on time in the insulations of the plugs under test.

The test had to be considered finished after either 100mA limit for leakage current had been met or the expected 168h of the endurance test had passed.

## 3.2 Design of the Setup

### 3.2.1 Current Measurement Concept Selection

Current measurement is generally an essential part of various electronics applications like battery management, variable frequency drives, fault detection, medical instrumentation and others, and the methods and technologies of current measurement significantly vary. Current measurement can be implemented using a shunt resistor, current

sense transformer, Rogowski coil, Hall sensor etc., all having their own advantages and disadvantages. The shunt resistor measurement technology was selected for the needs of this work due to its simplicity, linearity and relatively low cost. [16.]

Most commonly a current measurement system consists of a shunt resistor, which naturally translates the current passing through it to the voltage across it following Ohm's law, an operational amplifier, which amplifies the voltage over the resistor, as usually the voltage over the shunt resistor is small compared to the resolution of ADC (Analog-to-Digital Converter), an ADC and a microcontroller, which receives data from the ADC and performs required calculations and control functions (see figure 12). [17,40.]

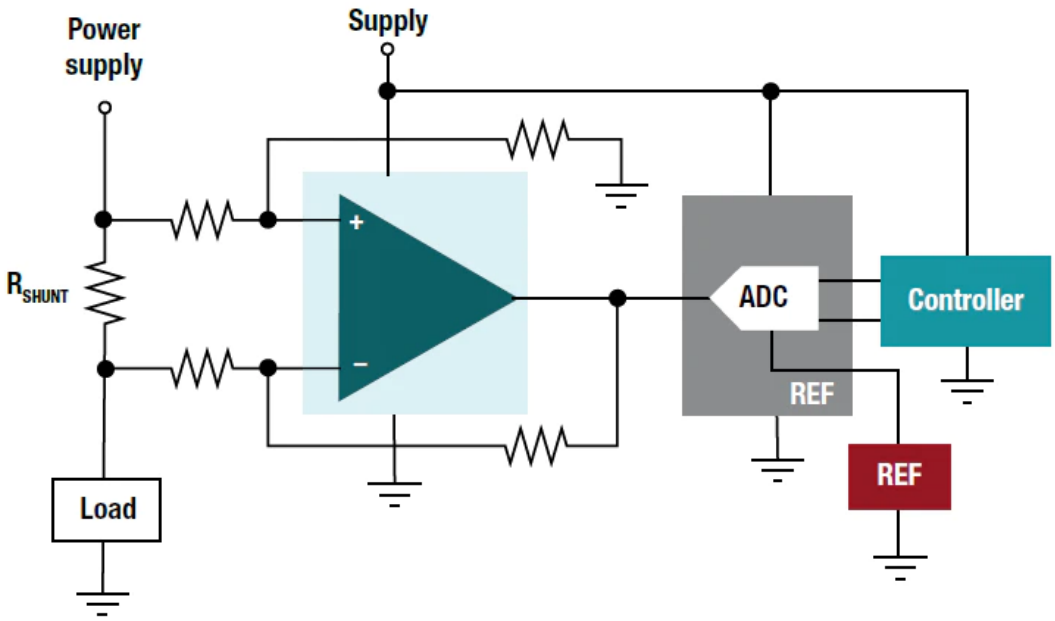


Figure 12. A general setup for current measurement. Copied from Texas Instruments Incorporated [17,40].

There are variations to operational amplifiers used for current measurement purposes. The simplest technique is to use a differential amplifier configuration with discrete resistors for the gain selection. However, this technique highly depends on the tolerances and temperature coefficients of an each individual resistor and can introduce measurement errors [18,2] and decrease the common mode rejection ratio of the operational amplifier, which is especially important if the measurement is done following the "high side"

method, meaning that the shunt resistor is placed straight after the power source, before the load, and is therefore potentially riding on a high potential [19] (see figure 13):

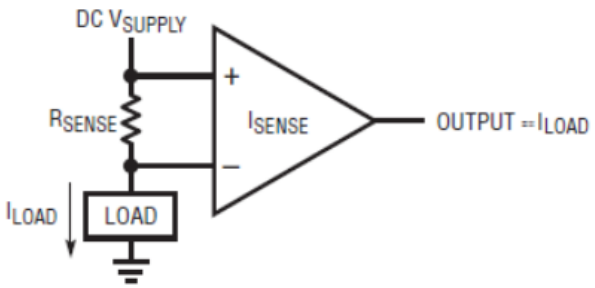


Figure 13. The high side current measurement configuration. Copied from Regan *et al.* [20,2].

To avoid such problems, there are ready-made operational amplifier solutions developed named current sense amplifiers, which have gain resistors laser trimmed and incorporated to the package to provide an increased measurement accuracy and reliability [21]. On top of that, there are even more integrated solutions available, which include also a shunt resistor and/or an ADC in one package in addition to the amplifier [17,5].

There are, however, some general challenges induced by the wide current range requirements of the given project. Namely, using single shunt resistor value and single operational amplifier gain value in practise means that neither low nor higher currents can be measured accurately: if single resistor is optimised for the mA range and, for example, has a value of 10Ω, the voltage developed across it in the uA range will be relatively small and will potentially be confused with the noise [17,7] and would also require a high-resolution ADC; otherwise, if the shunt resistor is optimised for the uA range and, for example, has a value of 1kΩ and a single gain is used, the voltage on the resistor in the mA range cannot be amplified without exceeding either amplifier input or output voltage limitations, as well as power limitations of a shunt resistor [17,7]. Therefore, one of the following solutions must be selected: either a shunt resistor has to be variable depending on the current passing through it, or the gain of the operational amplifier has to be variable depending on the input voltage it amplifies. Riedel and Schwarzbach [22] illustrate the described situation for a 50nA – 50A measurement range, which significantly exceeds the requirements of the current project yet provides a clear overview: with a variable-shunt solution currents of wide ranges can be detected with a single gain

setting, whereas with a variable-gain solution the lowest currents require a significantly higher gain, see figure 14:

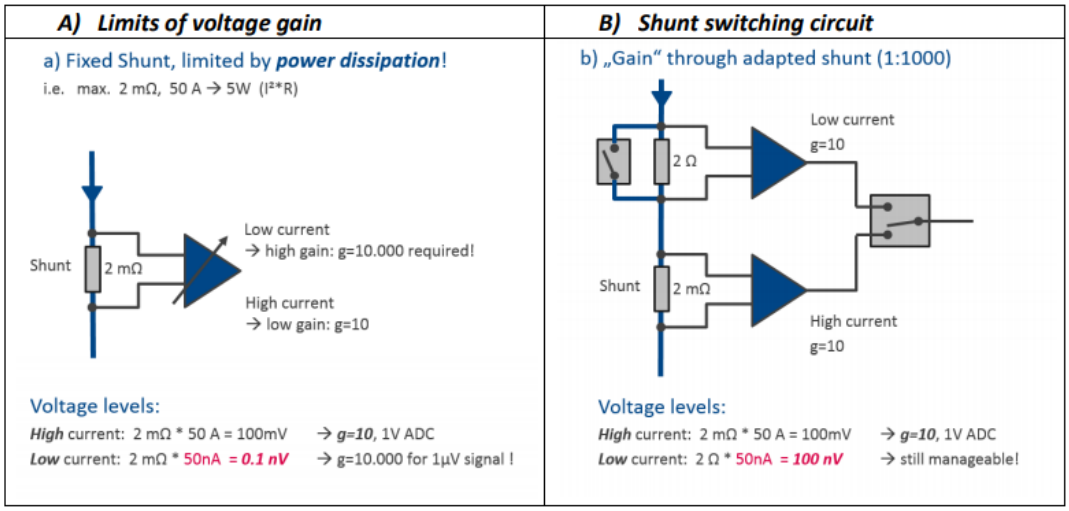


Figure 14. Two approaches to measuring wide ranges of input current. Copied from Riedel and Schwarzbach [22,3].

Riedel and Schwarzbach [22] also point out that current-dependent shunt resistance switching during current measurement should be precisely controlled in order to avoid a voltage drop on the load during sudden load current increase events. [22,7.]

The variable gain current sense amplifier solution was at the end preferred for the project to avoid any possible effects on the load, that is, the DC plug insulation, as the 50uA – 100mA range allows for reasonable gain settings even for low currents.

There is a range of criteria that need to be generally considered when selecting an amplifier for current sensing application:

- common-mode rejection ratio (CMRR) has to be considered when high side measurements are made, since CMRR introduces voltage offset errors on the output of the amplifier [23];

- common-mode range specify the common mode voltage that inputs of the amplifier can handle, for the low side measurements is it important that common-mode range also extends to negative voltages [24,6];

- Gain error and gain drift with temperature [18,2];

- Offset voltage on the input, offset voltage drift and input bias current, which introduce errors on the input of the amplifier [24,14].

Considering low current measurement requirements of the project, input offset voltage was amongst the most important criteria in the current sense amplifier selection. The operational amplifier itself was not expected to be subjected to temperature fluctuations, therefore drift parameters were for the most part ignored. Common-mode rejection ratio (CMRR) was also ignored for the most part as the low side measurement was used and the current measurement was planned to be introduced in series with a negative wire in-between the load (DC plug) and the ground. Overall, input offset voltage, gain error and extensive gain variability served as an input for the selection of the amplifier.

Texas Instruments PGA281 current sense amplifier was selected for the project purposes. PGA281 has a variety of configurable gains ranging from 1/8 to 176, low offset voltage depending on a gain (maximum (±20+235/G)uV, being approximately ±21uV when G = 176), gain error of maximum 0.15% and a fully differential rail-to-rail output. Offset current of the amplifier is also in a nA range. Gain setting is done via five digital input pins: G4:G0 (low level 0.1 – 0.2*DVDD*, high level 0.8*DVDD* – *DVDD*, *DVDD* – supply voltage for the amplifier digital circuitry) following the table presented on figure 15 below [25]:

| G3:G0 | G4 = 0 | G4 = 1 |
|---|---|---|
| 0000 | 0.125 | 0.172 |
| 0001 | 0.25 | 0.344 |
| 0010 | 0.5 | 0.688 |
| 0011 | 1 | 1.375 |
| 0100 | 2 | 2.75 |
| 0101 | 4 | 5.5 |
| 0110 | 8 | 11 |
| 0111 | 16 | 22 |
| 1000 | 32 | 44 |
| 1001 | 64 | 88 |
| 1010 | 128 | 176 |
| 1011 | Reserved(1) (0.125) | Reserved(1) (0.172) |
| 1100 | Reserved(1) (0.125) | Reserved(1) (0.172) |
| 1101 | Reserved(1) (0.125) | Reserved(1) (0.172) |
| 1110 | Reserved(1) (0.125) | Reserved(1) (0.172) |
| 1111 | Reserved(1) (0.125) | Reserved(1) (0.172) |

(1) Reserved for test-modes. Default gain in parenthesis.

Figure 15. Gain setting of the amplifier. Copied from PGA281 datasheet [25,6].

PGA281 consists of several blocks as shown on figure 16 below**.** Two symmetrical input amplifiers have their own supply voltage in a range of ±18V (VSN – VSP), allowing for a high common-mode voltage range, and the output amplifier has its own supply voltage VSON – VSOP of 2.7 – 5V range, which can be connected to DVDD digital power supply and referenced to the further circuitry analysing the output signal. [25.]

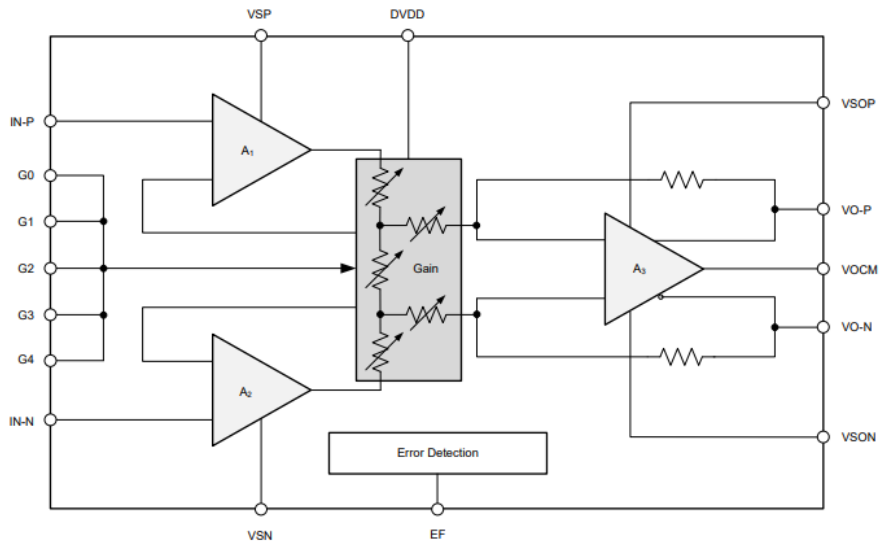


Figure 16. Simplified schematics of the amplifier. Copied from PGA281 datasheet [25,13].

The selected amplifier normally has a differential output voltage with the DC offset specified by the voltage externally supplied to the VOCM port, being mid-VSON-VSOP-supply according to the application information, to allow for the full output scale, as shown on figure 17 below. In such configuration the VOCM voltage does not have to be precise. [25.]

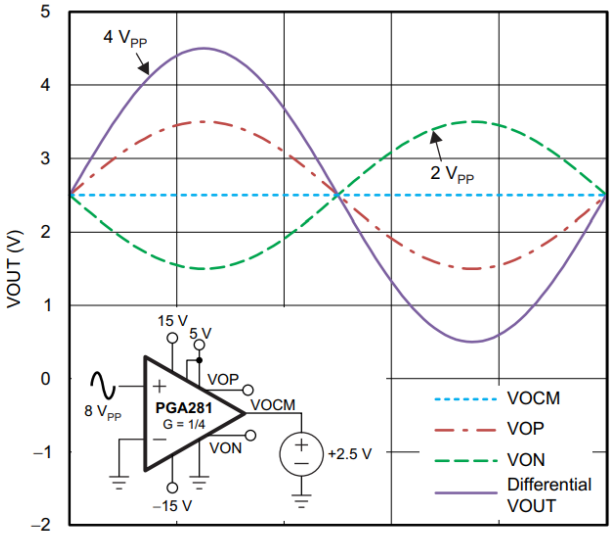


Figure 17. Differential output voltage of the PGA281 amplifier. Copied from PGA281 datasheet [25,15].

Described PGA281 features had to be accounted for in the overall setup planning, as described further.

### 3.2.2 Setup Overview

Refined by the current measurement considerations presented above, the general idea of the project setup operation was as follows: the possible leakage current in the plug emerging during THB test flows through a single both for uA and mA ranges shunt resistor inserted in-series with the plug's negative wire. The input voltage on the shunt resistor is then amplified by a PGA281 amplifier and interfaced to the Arduino Mega2560's ADC. The shunt resistor and current amplifier related circuitry is placed on a separate PCB. Arduino processes the digital value received, controls the gain selection through digital I/O pins, detects maximum and minimum currents measured per second, averages all

measured values per second and reports the results to the PC through the serial port using TeraTerm terminal. TeraTerm script then executes documentation of the recordings with a time stamp to the .txt file on the PC. The overall picture of the test setup is presented on figure 18:

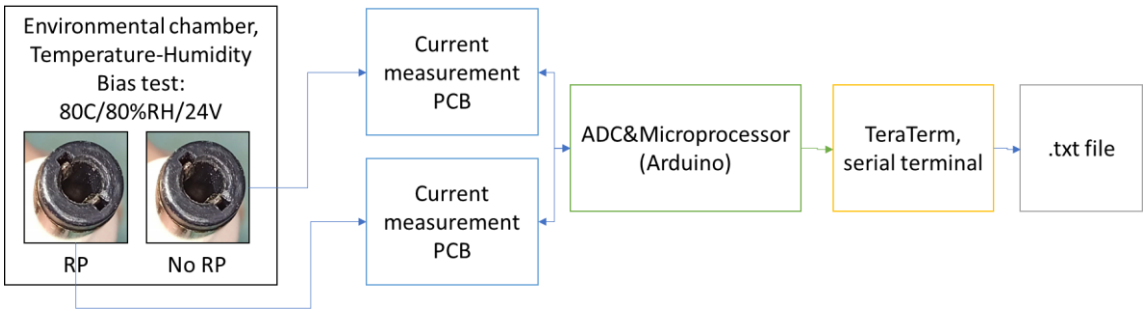


Figure 18. Measurement setup overview.

As specified by requirements, both not containing red phosphorus and red phosphorus containing plugs had to be subjected to the same test conditions simultaneously, therefore two current measurement PCBs were included in the setup presented above. Alternatively, one PCB could have been designed providing current measurement functionality for both plugs, however this possibility had not been explored in the current work.

### 3.2.3 Current Measurement PCB Schematics

Datasheet application information [25], *TI Precision Designs: Verified Design 10 µA – 100 mA, 0.05% Error, High-Side Current Sensing* by Ian Williams [26] and PGA281 Evaluation Module's User's Guide [27] were highly referenced in the PCB design of the project and some parts of the circuitry were borrowed directly as:

- input 10kHz filter configuration shown on figure 19 was borrowed from the Verified Design presented by Ian Williams [26] as the project did not have precise requirements related to the input filtering:

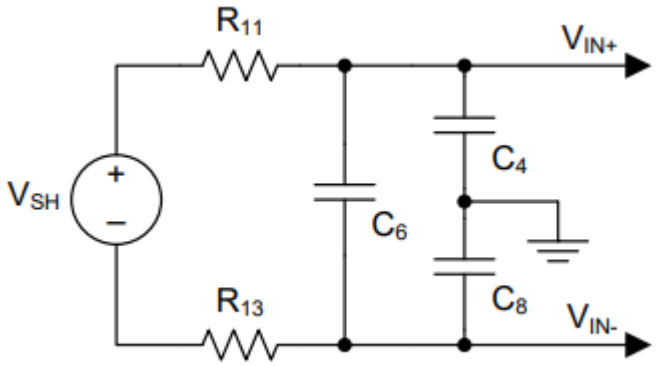


Figure 19. Input filter configuration for PGA281. Copied from Williams [26,5].

- power supplies protection circuitry design and components were borrowed from Verified Design presented by Ian Williams [26,19] (see complete schematics of the project in Appendix 1).

- RC bypass filters (22Ω/470nF) of power supplies were also inserted following datasheet recommendations. [25,21.]

However, some parts of the circuitry differ from the designs presented in the datasheet and verified designs documents. First, since Arduino ready-made analogRead() function does not support differential inputs for the ADC, and other possibilities of accessing ATmega2560 (microcontroller used by Arduino Mega 2560) differential ADC inputs were not explored at the time, the simplest solution seen was to configure the output of the current sense amplifier to the single-output configuration. In this configuration, the output voltage, being thus between the single positive output (VOP) and the ground (VSON) pin, has a DC offset of VOCP voltage, and is a half of the output voltage expected in the normal differential-mode operation (refer to figure 17, VOP curve), and therefore requires a compensation in the appropriate design calculations. Also, configuring the current sense amplifier in a single-output mode requires a stable and precise VOCM voltage, as otherwise the reference will create additional errors to the output voltage measurement on top of the output offset voltage error of maximum ±120uV for the single-output mode specified by the datasheet [25].

An output filter was inserted according to the datasheet recommendations (see figure 20).

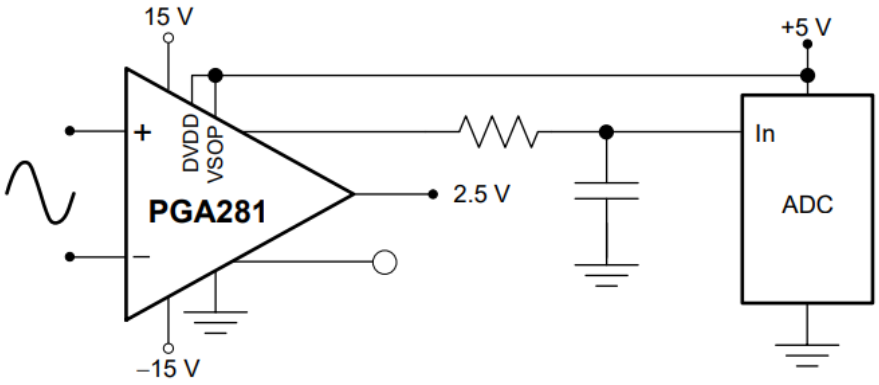


Figure 20. A single-output configuration of the current sense amplifier. Copied from PGA281 datasheet [25,18].

Arduino's internal ADC of 10 bits resolution was used for the project purposes. However, the Arduino 5V line, which is normally used as a high limit reference for the ADC, in the current project setup receives power via USB and might not be accurate and stable, creating thus an additional uncertainty to the measurement result if used as such for the ADC reference.

With purposes of creating a precise and stable voltage for the VOCM input and for the ADC reference, KA431SLMF2TF Programmable Shunt Regulator was used (the component was recycled from the KaVo Kerr proto board and that was the main reason for component selection). The component has a Vref pin (see figure 21) of 0.5% tolerance in a 2.482…2.495…2.508V range [28] and therefore it was directly connected to the VOCM pin of the current sense amplifier. The component was used in the following configuration presented in the datasheet (see Figure 21):

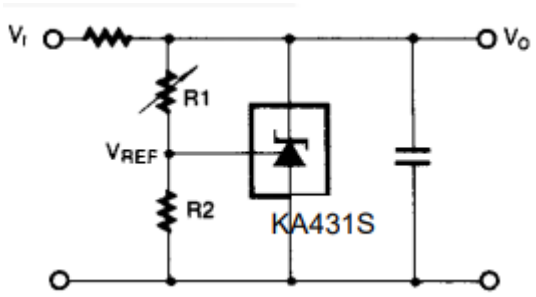


Figure 21. Regulator application example. Copied from KA431SL datasheet [28,5].

Set R1=27kΩ and R2=36kΩ allow for an ADC reference voltage Aref in a range of a 4.365...4.516V (the exact voltage depends on resistor tolerances, the actual Vref voltage and Vref pin input current). This gives a more defined ADC code width (1LSB) of Aref/1024 being 4.263…4.410mV. The ADC reference thus achieved was also used as a VSOP and DVDD supply for the current sense amplifier (refer to figure 16) in order for the ADC reference and the output amplifier ranges to be compatible. Thus, by design the ADC reference is fed back to Arduino and Arduino is programmed such that the external ADC reference is used (see full schematics in Appendix 1 and Arduino code in Appendix 3).

The input circuitry of the whole PCB (presented on figure 22) was built such that the whole PCB was meant to be in series with the plug's negative wire, and so the wires were planned to be soldered to the PCB as the simplest connection possible. Input line is controlled by an N-channel MOSFET IRFL4310PBF (also the component recycled from the KaVo Kerr proto boards) by Arduino's digital output such that when 100mA current is detected, the MOSFET is turned off and the current flow is stopped. In addition, a 125mA fuse was inserted on the input line to provide additional means of protection if other means of current restriction fail.

The input line was overprotected to ensure that possible leakage current would not under any circumstances exceed a critical value and cause fire.

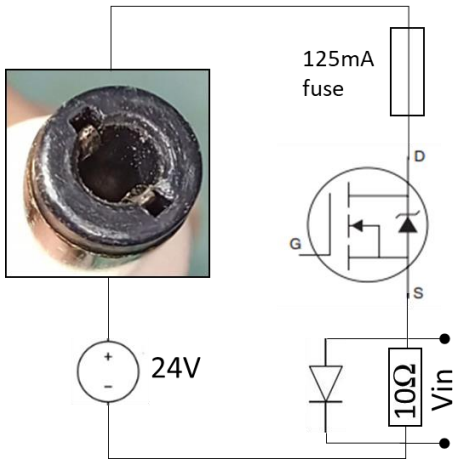


Figure 22. Input circuitry connections.

A shunt resistor of 10 Ohm 0.5% 1W KOA Speer Current sense resistor was used for the application. Resistor value of 10 Ohm was seen optimal for both mA and uA ranges: with 50uA current, the voltage on the shunt resistor is 500uV, which is significantly higher than input offset voltage (around 21uV for a 176 gain [25], which gives a 4.2% error), and with the highest 100mA current the voltage on the resistor is 1V and power is 0.1W which is well within specifications.

A diode BYV27-200-TAP was used as a shunt diode in parallel with a shunt resistor to leverage the effect of transients, as it was expected that the red phosphorus induced failures might generate sudden short circuits. The diode has forward voltage of 1.07V maximum [29], which was the reason for its selection (and the component was also re-cycled from proto boards).

LEDs were used for indicating a selected gain, a MOSFET state and to highlight a current sense amplifier error condition (EF LED), as the current sense amplifier has a specific pin to indicate error condition. The error pin was not wired to the Arduino in the current project setup, since this feature was not taken advantage of.

Banana plugs were used for supplying power rails and the ground to the PCB: +15V, -15V and GND. As it was already described, the power for the output part of the current sense amplifier is supplied via Arduino (and Arduino receives power from the PC via USB) and regulated through the shunt regulator as described above.

PCB schematics was built using EasyEDA PCB software and it is presented in Appendix 1.

### 3.2.4 Layout

The layout was made such that there are only 2 layers – top and bottom and the ground was distributed all over as a copper plane.

Bypass capacitors were placed as near as possible to the power lines they are placed across in the design, for example circuitry related to the VOCP (2.5V reference) and the power supply for the output part of the current sense amplifier were placed on the bottom

of the board almost directly under the chip and vias were placed as close to related pins as possible.

Connectors for analog signals were placed separately from connectors for digital signals and as close to the chip as was seen reasonable.

There were small +15V and -15V copper areas made on the top layer of the layout leading directly to the appropriate supply pins of the chip.

Kelvin connection, that is, the connection with four traces, where two are used for delivering current and two are used for voltage sensing [17,4], was used for the shunt resistor connection even though for low current measurements it is not critical.

Generally, components were situated as close to the related circuits as possible and recommended pad dimensions in datasheets were implemented where applicable.

Also, there were multiple ground vias placed to improve the connection between ground planes on top and bottom layers.

The layout of the PCB and gerber files for manufacturing were also made in EasyEDA software and supplied to the PCB manufacturing company. Components were then assembled manually with an aid of solder flux and solder paste.

The layout and the bare PCB photographs are presented in Appendix 2. The assembled PCB (PCBA) is presented on figure 23 below:

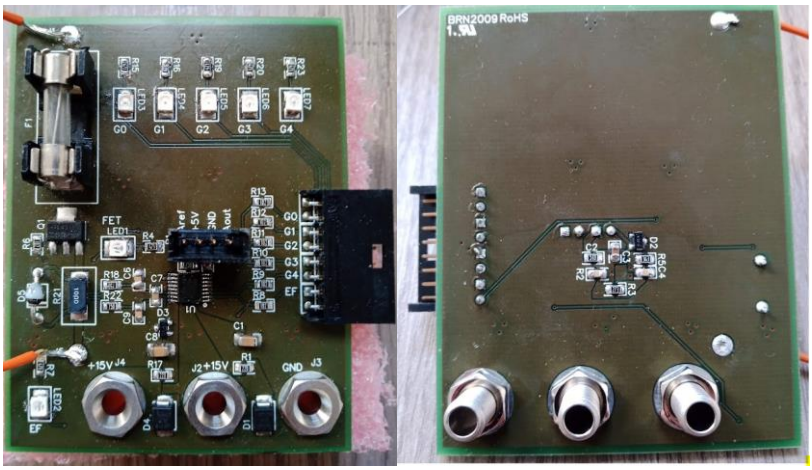


Figure 23. PCB with components assembled, top and bottom sides.

### 3.2.5 Control and Data Processing

In this project Arduino Mega2560 (that is, Atmel ATmega2560) performs the control of the gain setting and a MOSFET control, provides the PCB board with 5V and GND, receives the Aref analog voltage regulated on the separate PCB for the ADC external reference and receives an Aout signal being a single-ended output voltage of the current sense amplifier. Altogether the PCB is referenced to Arduino through six digital I/O pins: five pins for gain setting G4:G0 and one for the FET control.

Arduino also calculates the average measured current value per second, detects maximum and minimum measured current values and communicates them via serial terminal.

Input voltage is calculated from the current sense amplifier output voltage as:

$$Vin = \frac{Vout}{G}. \tag{2}$$

If only the shunt resistor alone had been used, the input current would have been calculated as $Iin = \frac{Vin}{R} = \frac{Vout}{R*G}$. However, since the diode is used in parallel with the shunt resistor, the conductance of the input is no longer linear, as the diode starts conducting current following the characteristic curve shown on figure 24 already at approximately

500mV. The dependency of the input current on the input voltage can thus be generally defined as:

$$I_{in} = f(V_{in}) = f\left(\frac{Vout}{G}\right). \quad (3)$$

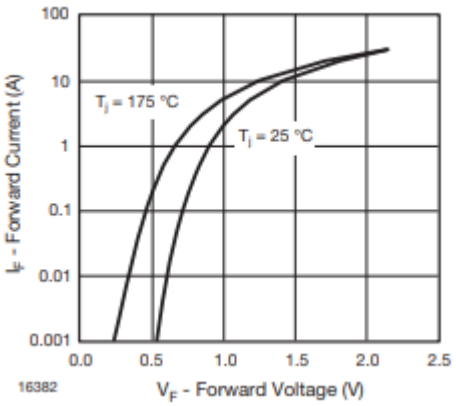


Figure 24. Characteristic curve of diode BYV27-200-TAP. Copied from BYV27 datasheet [29,2].

$Vout$ can be calculated from the ADC value measured by Arduino as follows:

$$Vout = \left(ADC_{measured} - ADC_{2.5v_{offset}}\right) * 1LSB * 2, \quad (4)$$

since as it was described above, in the single-output configuration the 2.5V reference offset is present on the single-ended output and the output itself is the half of the normal differential mode output.

Substituting the formula (4) to the current measurement formula (3):

$$I_{in} = f(V_{in}) = f\left(\frac{\left(ADC_{measured} - ADC_{2.5v_{offset}}\right) * 1LSB * 2}{G}\right). \quad (5)$$

Averaging of the measured current can be further calculated as:

$$I_{in\_avg} = \frac{\sum_i^n I_{in_i}}{n} = \frac{\sum_i^n f\left(\frac{\left(ADC_i - ADC_{2.5v_{offset}}\right) * 1LSB * 2}{G_i}\right)}{n}, \quad (6)$$

where n – the number of current measurements per second.

However, in the actual project $I_{in\_avg}$ was calculated as:

$$I_{in\_avg} = f\left(\frac{1LSB*2*\sum_i^n \frac{\left(ADC_i - ADC_{2.5v_{offset}}\right)}{G_i}}{n}\right) = f\left(V_{in_{avg}}\right), \quad (7)$$

which is incorrect and which must have contributed to the measurement errors in the final verification.

In the actual project, the current sense output voltage measurement reading and summing of $\frac{\left(ADC_i - ADC_{2.5v_{offset}}\right)}{G_i}$ was being looped for a second and the average current value was calculated only after the second had passed following the formula (7). Also, a running average of 10 latest $ADC_i$ values was being constantly calculated inside the loop to avoid switching in case the measurement value would accidentally peak. Gain switching decisions inside the loop were being made based on a gain, $ADC_i$ value, running average value and the threshold defined for the range.

The dependency $I_{in} = f(V_{in})$ had to be investigated prior to specifying range thresholds and gain settings. Two high-precision Keithley 2000 Series multimeters were used for the task: one for measuring current flow through the resistor-diode pair and second for measuring voltage on the resistor-diode pair. Power supply was used to supply variable current for testing (see figure 25 for the setup overview). The results collected were interpolated in Excel to arrive at the conductance dependency $I_{in} = f(V_{in})$ (see results summary and Excel graph on figure 26). Polynomial coefficients are presented on the graph in a shortened form for convenience, the actual values have 30 digits precision and 8-digit precision values were included in a code to minimize errors (Arduino's float accuracy is 6 – 7digits).

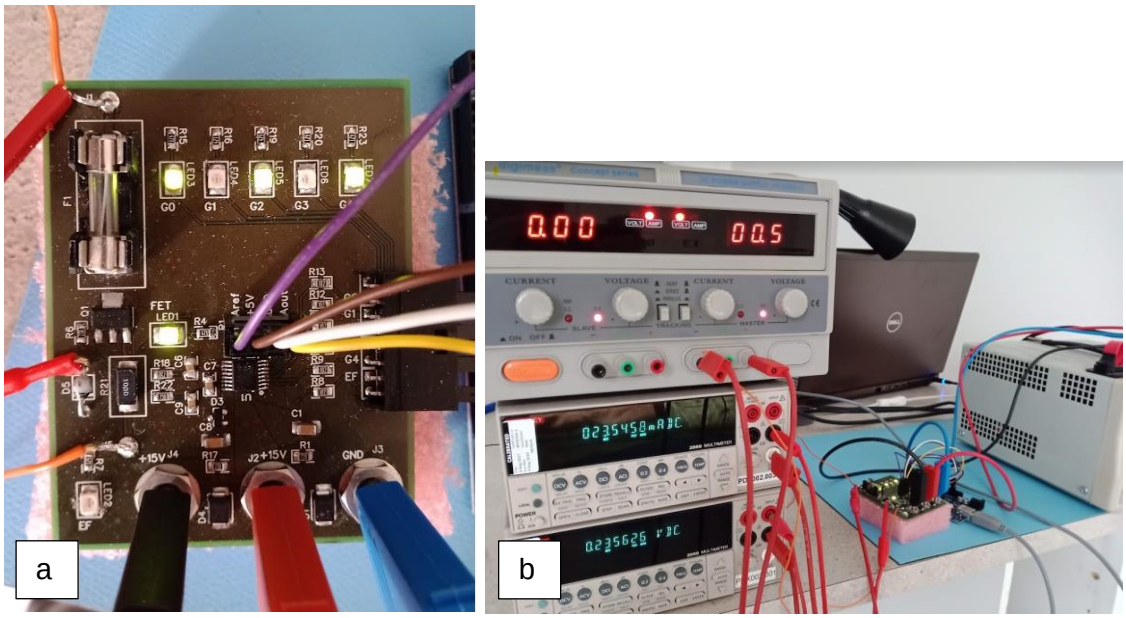


Figure 25. Conductance dependency study setup: a) measurement PCB: current measuring multimeter was connected in-series with input, voltage measuring multimeter was connected in parallel, across the diode; b) overall setup with power supply and multimeters used.

| mV | mA |
|---|---|
| 0,7000 | 0,0700 |
| 1,074 | 0,1078 |
| 1,521 | 0,1251 |
| 3,045 | 0,3045 |
| 10,012 | 1,0012 |
| 15,500 | 1,5510 |
| 67,950 | 6,7960 |
| 246,400 | 24,6600 |
| 317,000 | 31,7200 |
| 411,300 | 42,2100 |
| 449,100 | 45,1600 |
| 489,800 | 50,0300 |
| 525,300 | 56,0400 |
| 555,400 | 64,5300 |
| 572,300 | 71,7500 |
| 587,800 | 80,5900 |
| 605,300 | 93,6700 |
| 612,300 | 100,6200 |

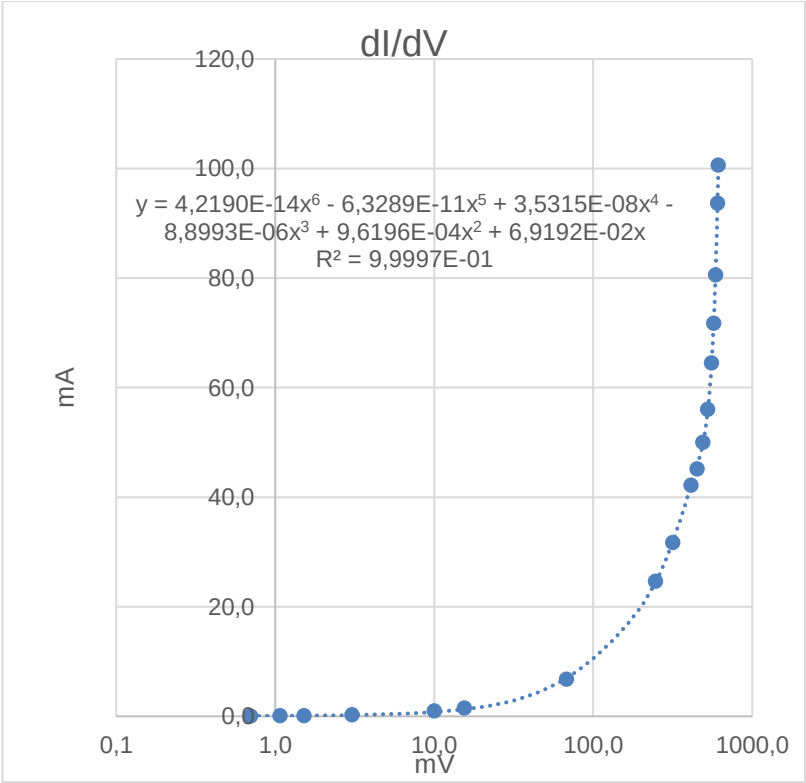


Figure 26. Conductance dependency investigation results: measurement table and a graph.

As seen from the results table presented on figure 26, the expected $V_{in}$ for $I_{in}$ = 100mA is around 612mV. Assuming 100mA is the highest limit for current measurement, mA range gain can be calculated based on formula (2) as:

$$G_{mA} \leq \frac{Vout_{max}}{Vin_{100mA}} = \frac{(Aref_{min} - Vref_{max}) * 2}{0.612V} = \frac{(4.365V - 2.508V) * 2}{0.612V} = 6.069. \quad (8)$$

The closest available gain from the table presented on figure 15 is 5.5. Based on formula (2), with 5.5 gain the smallest $V_{in}$ that can be detected corresponds to:

$$V_{in\_min} = \frac{Vout_{min}}{5.5} = \frac{1LSB_{min} * 2}{5.5} = \frac{4.263mV * 2}{5.5} = 1.55mV, \quad (9)$$

that is, 155uA. For the uA range the highest possible gain of 176 was selected to allow for the maximum amplification. Similarly, gain 176 specifies the maximum possible $V_{in}$ for the range as:

$$V_{in\_max} = \frac{Vout_{max}}{176} = \frac{(Aref_{min} - Vref_{max}) * 2}{176} = \frac{(4.365V - 2.508V) * 2}{176} = 0.021V, \quad (10)$$

which corresponds to 2.1mA.

Thus, the absolute limitations of the ranges are: mA – from 155uA to 100mA; uA – from 50uA (in practice, lower, not calculated) to 2.1mA.

The hysteresis current range of approximately 1.5mA was selected in attempt to prevent the circuitry from the unnecessary switching: the uA gain has to be switched to the mA gain when input current approaches 2.1mA and the mA gain has to switch to the uA gain when input current approaches 0.6mA.

To proceed, first the ADC offset value of 577 was measured with no current passing through the input, such that the output would be only the expected 2.5V reference offset. Further ADC digital values of 993 when G = 176 and 580 when G = 5.5 were selected for the threshold values. Substituting formula (4) into formula (2), 993 value corresponds to:

$$V_{in} = \frac{(993-577)*4.263*2}{176} = 20.152mV, \quad (11)$$

which corresponds to 2.01mA and 580 value corresponds to:

$$V_{in} = \frac{(580-577)*4.263*2}{5.5} = 4.651mV, \quad (12)$$

which corresponds to 465.1uA.

It is initially assumed that the current is in a uA range and so the uA gain of 176 is set as a default. Gain setting is then being changed inside the 1000ms voltage reading loop if the four conditions are met: the present state gain setting correct for the threshold applied; $ADC_i$ exceeds/falls below the set threshold; $ADC_i$ is higher/lower than the running average of last 10 measurements; the running average exceeds/falls below the threshold, see figure 27 below for simple visualization:

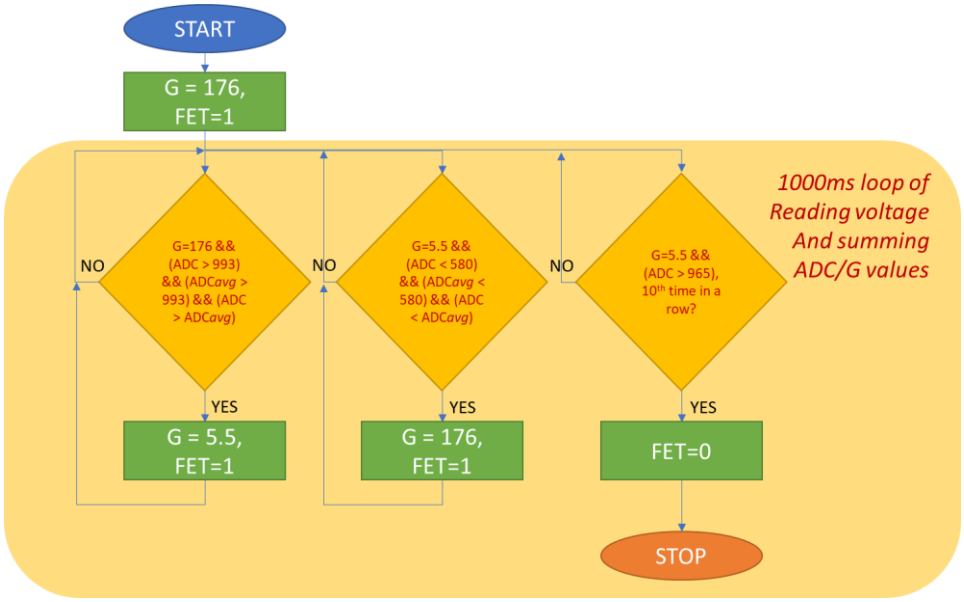


Figure 27. Simplified block diagram of the code representing switching conditions.

ADC processing of analog voltage takes approximately 100us, as defined by the fact that Arduino analogRead() configuration for the ADC clock is 125kHz and the normal ADC conversion takes approximately 13 clock cycles [30;31]. The time required for the amplifier to re-select the gain is specified in the datasheet as “settling time” and is maximum 40us [25], therefore whenever the switching condition occurs, a delay of 100ms is

introduced in the code. The delay of 100ms is redundant and can be reduced to approximately 100us.

The stop condition is such that the output pin controlling the FET is set high by the code when the corresponding to 100mA current ADC value is being detected ten readings in a row, as visualized on the figure 27 above. The required ADC value of 965 was also specifically measured with current sense PCB being supplied input current of 100mA.

The microcontroller also records maximum and minimum measured values for each second. TeraTerm serial terminal was used for communication with Arduino during the actual test, since it enables running macro scripts for, for example, recording the values provided by Arduino serial terminal to the text file. A script was configured such that it added also a timestamp to each set of received values (the script is presented in Appendix 3 after Arduino code).

There was a separate measurement PCB board for each plug: red phosphorus containing one and not containing one, therefore additional set of 6 I/O pins, 5V and GND and analog input were used for the second board. Aref pin of the second board was left unconnected. VOCM reference voltage was measured and the result was the same for both boards being 2.502V, therefore no additional error from Vref difference was expected. Leaving Aref pin unconnected did not interfere with the accuracy of the second PCB board measurement.

The code was practically duplicated for analyzing the measurement of the second analog input.

### 3.2.6 Accuracy Estimation

The factors that were recognized and estimated to contribute to the accuracy of the result of the current measurement, as well as their possible effects are listed in the table 1 below:

Table 1. Accuracy estimation. Some data gathered from ATMega2560 datasheet [31] and PGA281 datasheet [25].

| Factor | Specified value | Significance for the design | Effect |
|---|---|---|---|
| Shunt resistor tolerance | 0.5% | Shunt resistor value ±0.05Ω | Introduces error of max 50uA in mA range, negligible in uA range as well |
| Input offset voltage | max ±(20+235/G)uV | ±63uV, G=5.5 (mA range)<br>±21uV, G=176 (uA range) | Effect in mA range negligible, in uA range introduces current measurement error of max ±4.2% at 50uA |
| Gain error | max ±0.15% | ±0.15% | Negligible for both measurement ranges |
| Output offset voltage (specified for single-ended amplifier configuration) | ±120uV for 1V/V, 1.375V/V gains<br>±3uV for 64V/V gain | Assumed ±120uV for G=5.5<br>Assumed ±3uV for G=176 | Negligible for both measurement ranges |
| ADC code width (1LSB) | Aref/1024 | 4.263…4.410mV | "Quantization error" of input voltage ±Aref/1024/G/2: ±388…401uV in mA range, error effect on measured current increases according to dI/dV curve<br>±24…25uV in uA range, that is, ±2.4…2.5uA current measurement error, means max ±5% at 50uA |
| ADC absolute accuracy | max 2.5LSB for Single Ended Conversion VREF = 4V, VCC = 4V, CLKADC= 200kHz | Assumed 2.5LSB = 10.658…11.025mV | Effect on Vin: (10.658…11.025mV)/G 1.938…2.005mV in mA range, error effect on measured current increases with dI/dV curve 0.061…0.063mV in uA range, error in measured current: 6.1…6.3uA means max 12.6% at 50uA. |
| ADC offset accuracy programmed in Arduino code | - | Single ADC code value 577 is assumed as constant offset representing VOCM 2.5V reference, but ADC absolute accuracy errors apply to it | *Effect not estimated separately* |
| ADC code width (1LSB) programmed in Arduino code | | Nearly average value of 4.328mV is involved in calculations which might differ depending on actual Aref | *Effect not estimated separately* |

| | | | |
|---|---|---|---|
| Inaccurate measurement of the average input current value | | Wrong formula used in the actual experiment. | *Effect not estimated separately* |

Timing delays and errors were not considered.

Overall, input offset voltage of the current sense amplifier and ADC-related factors, like ADC code width and ADC absolute accuracy are amongst the biggest intrinsic to hardware error sources. In addition, errors were introduced by using set ADC offset value and set ADC code width in calculations in the Arduino code. Also, as it was described already, the wrong formula (7) was used for the average current measurement value calculation in the actual test instead of the correct formula (6).

Based on the accuracy estimation presented, the biggest errors were expected in the lowest current measurements' results, and the errors were expected to increase in the highest current measurement results due to the nonlinearity of the input conductance dependency $I_{in} = f(V_{in})$ measured.

### 3.2.7 Setup Verification and Errors

Error calculation and compensation for errors in measurement were done post-factum in Excel due to practical schedules of the project and the need to conduct the actual test as soon as possible. Another possibility could have been to add the compensation for errors to the microcontroller code already such that the values recorded had already been correct.

Keithley 2000 Series multimeter set up for current measurements and power supply were used to conduct the final verification and error calculation of the setup (see figure 28 below). Power supply supplied the current into the measurement PCB input, which was measured by the multimeter, and the current was then compared to the calculated values provided by the Arduino through the serial port. Actual tables are presented in Appendix 4.

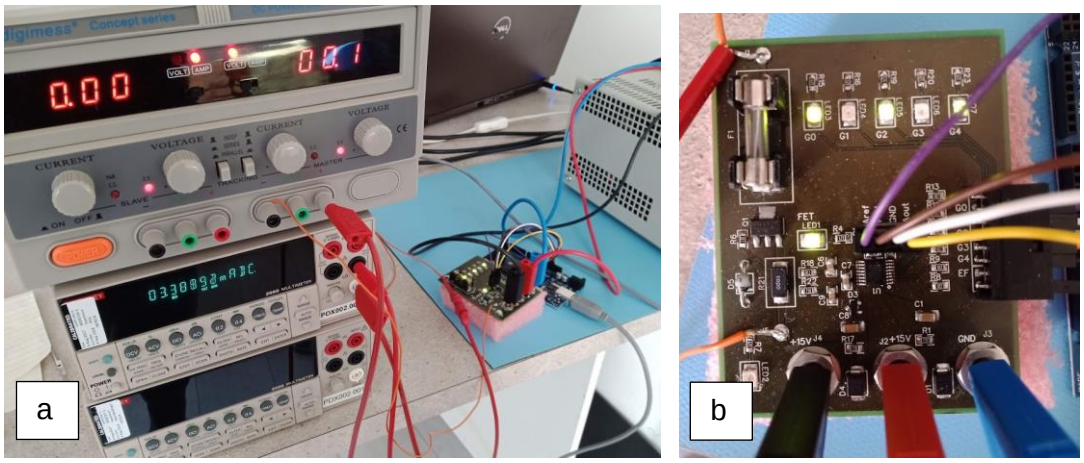


Figure 28. Final verification setup: a) power supply and multimeter used in verification; b) measurement PCB: multimeter was connected in series with the input (red clip).

Error % was calculated as follows:

$$Error\ (\%) = \frac{|Iactual - Imeasured|}{Iactual} * 100\%, \quad (13)$$

As presented on figure 29, error distribution in the uA range takes a logarithmic form starting from approximately 45% and decreasing to approximately 15%:

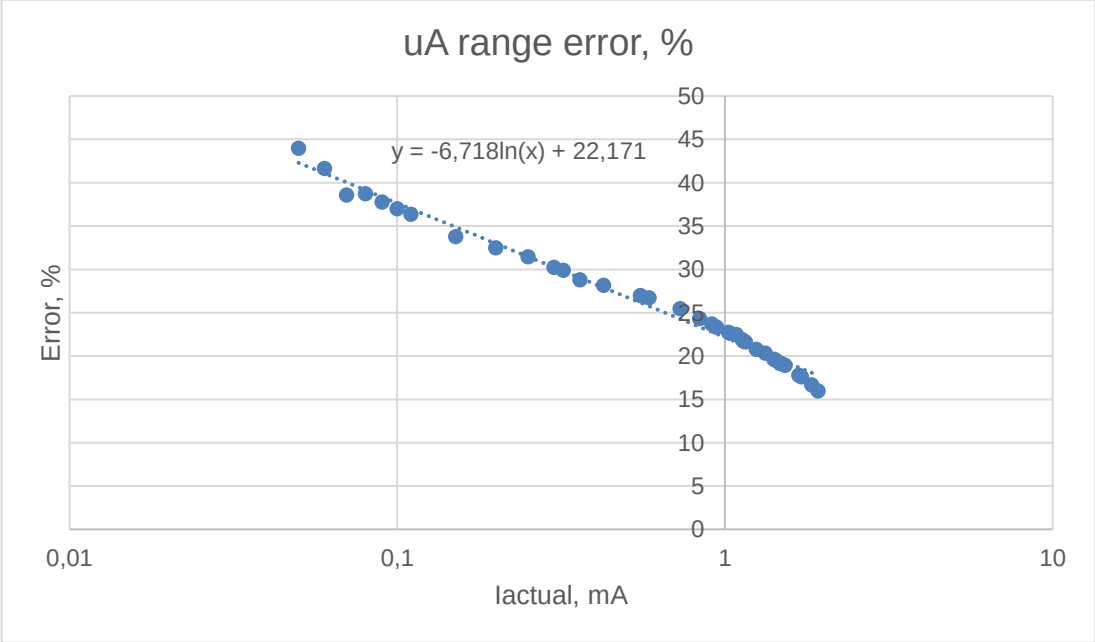


Figure 29. Measured error distribution in the uA range.

In the mA range, the calculated error follows logarithmic form up to around 7mA and then from approximately 45mA, as presented on figure 30:

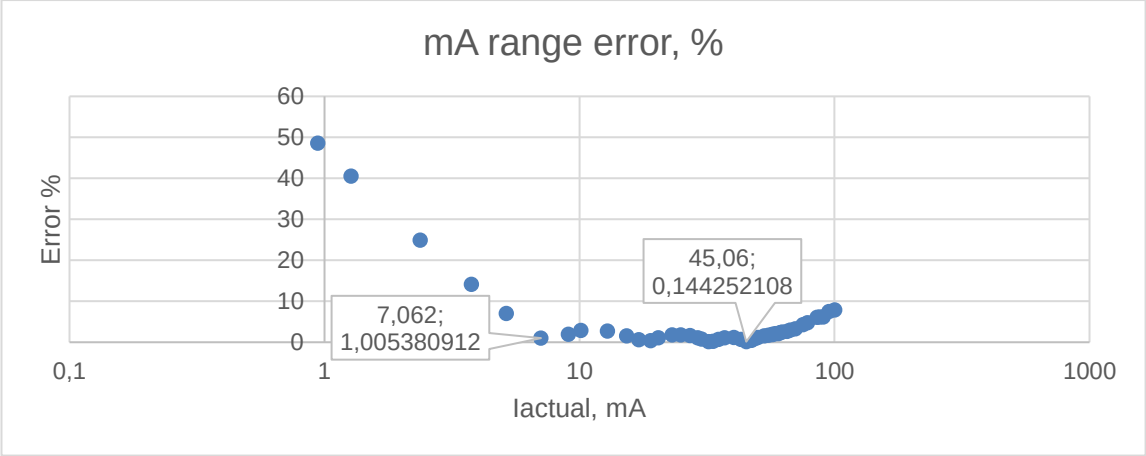


Figure 30. Measured error distribution in the mA range.

To allow for reliable measurements, a calibration was needed for both ranges. Given the data, the most convenient way of calibration identified was to recalculate the actual current measurement values following the procedure:

$$I_{actual} = I_{measured} + f(I_{measured}), \quad (14)$$

where $f(I_{measured})$ was defined as the dependency of $|Iactual - Imeasured|$ on $Imeasured$ and was calculated in Excel in practice. For the uA range, $f(I_{measured})$ is presented on figure 31:

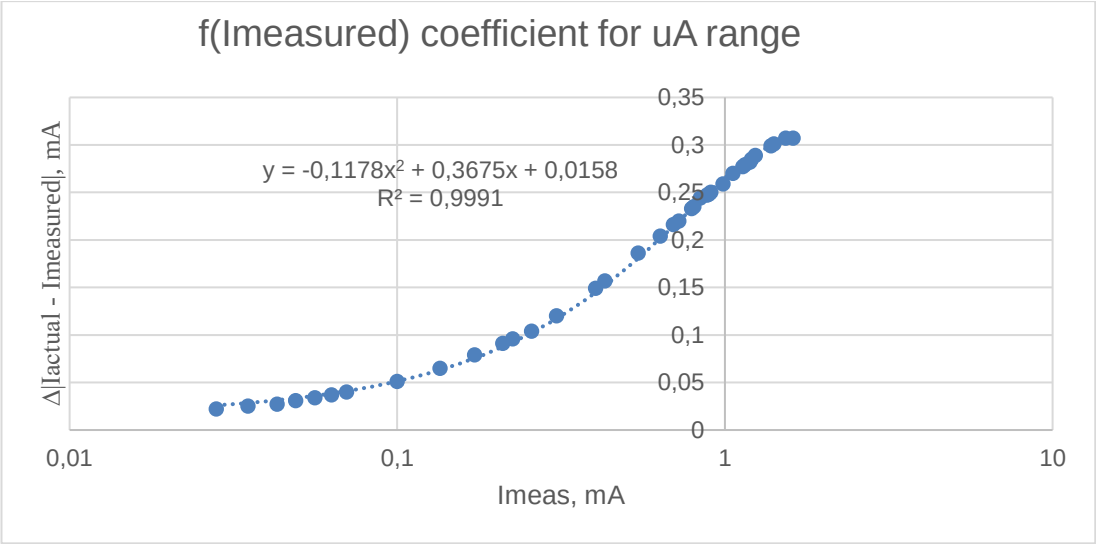


Figure 31. $f(I_{measured})$ equation for the uA range. The equation is rounded for convenience purposes, actual coefficients have 30-digit accuracy.

The suitable equation for the mA range is presented on figure 32:

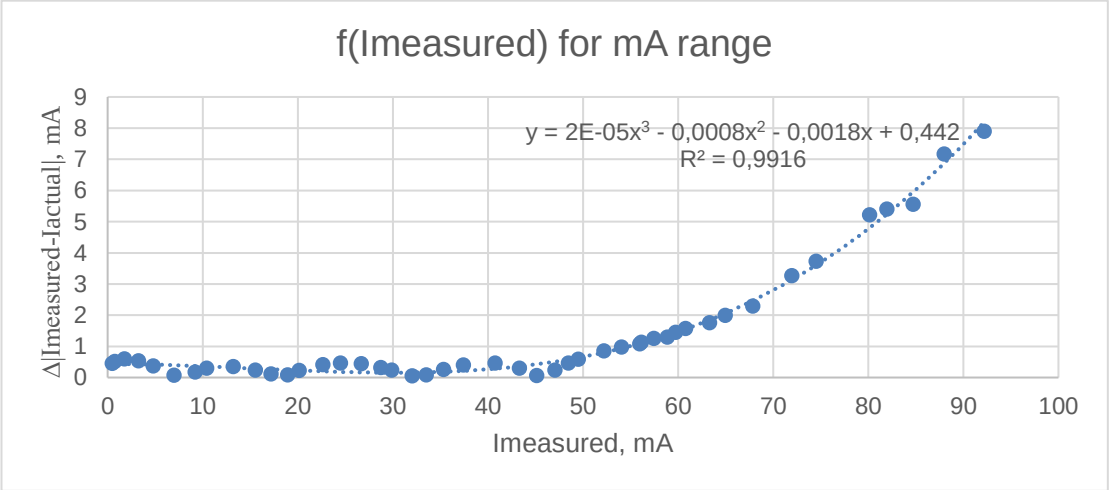


Figure 32. $f(I_{measured})$ equation for mA range. The equation is rounded for convenience purposes; actual coefficients have 30-digit accuracy.

The measurement results received during the test were thus compensated using above-mentioned formulas for the final presentation.

## 3.3 Actual Test

For the actual study, the DC plug was connected to the measurement PCB in the following way (in-series with the negatrive wire) as shown on figure 33 below:

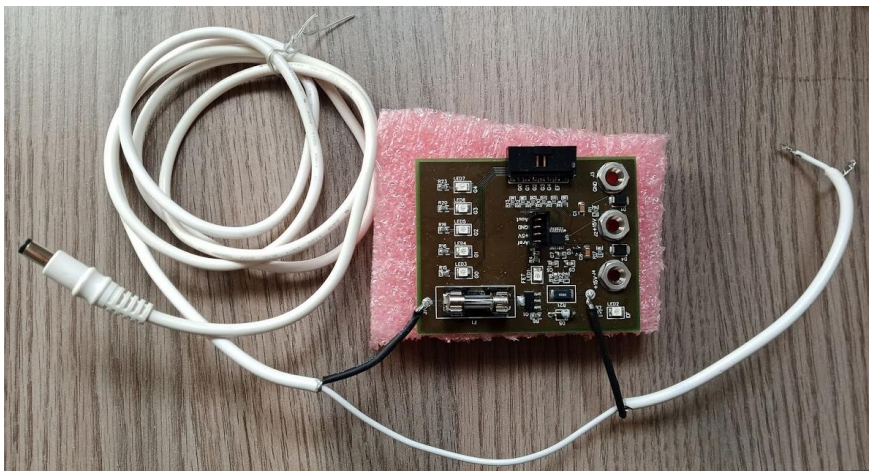

Figure 33. Final plug-PCB connection – the PCB is in-series with the negative wire.

The actual test was conducted using an environmental chamber such that plugs were inserted and powered by an external power supply (24V) (refer to figure 34, 24V power supply). Conditions for the test were 80ºC/80%RH. The current measurement PCB was powered by another power supply (refer to figure 34, 15V power supply, not shown fully). Both current measurement PCBs were connected to the Arduino and Arduino was communicating with the PC via TeraTerm terminal, which was logging current measurement values into the text file.

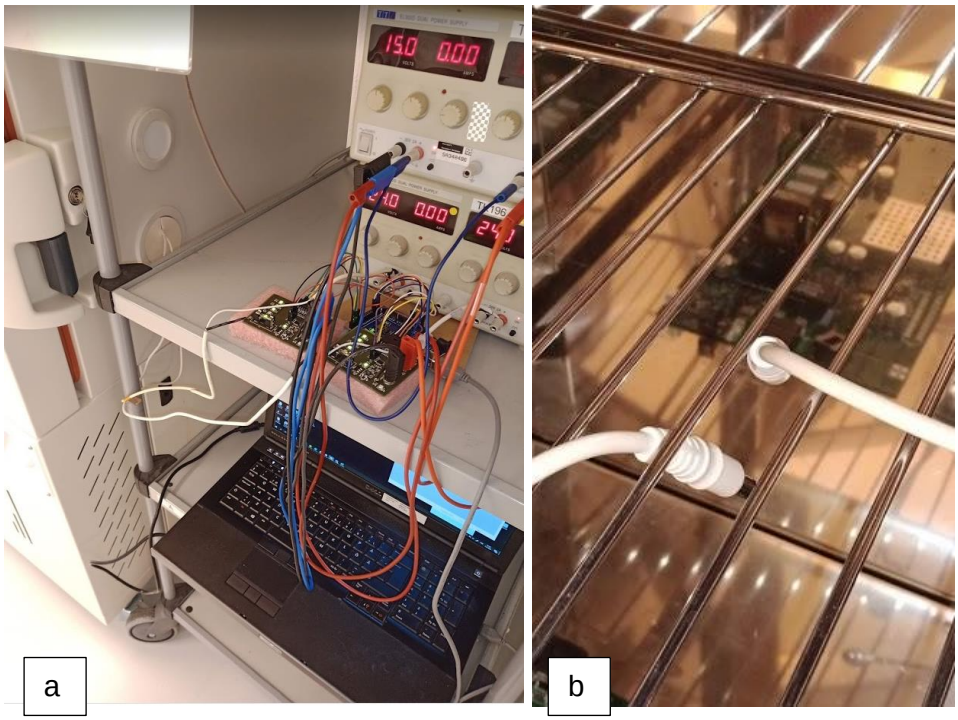


Figure 34. Test setup overview: a) external to the environmental chamber setup; b) two plugs inserted into the environmental chamber.

Altogether three red phosphorus containing plugs were tested in the environmental chamber. First plug was under test overnight for approximately 13h and then the test stopped due to the leakage current reaching 100mA value. After that, the same plug was tested for the second time for 50min and then the test was stopped, as the leakage current had reached 100mA value.

Then, second plug was put under the test for a limited amount of time (11min) to observe the current behavior in the beginning of the THB test. The test was stopped voluntarily.

Finally, third plug was put into the environmental chamber and the test was stopped in approximately 50min due to the leakage current 100mA limit.

## 4 Results

As the result of the work, the setup for measuring and registering possible leakage currents in the DC plug insulation induced by red phosphorus flame retardant failures was

built. The setup was verified against the actual current measured with the Keithley 2000 Series multimeter and the measurement results' calibration procedure to reduce setup errors was determined and presented.

Next, three plugs were tested in the environmental chamber. Below is the graph for the average leakage currents measured during Test 1, each data point corresponds to the average leakage current measured per second (see figure 35):

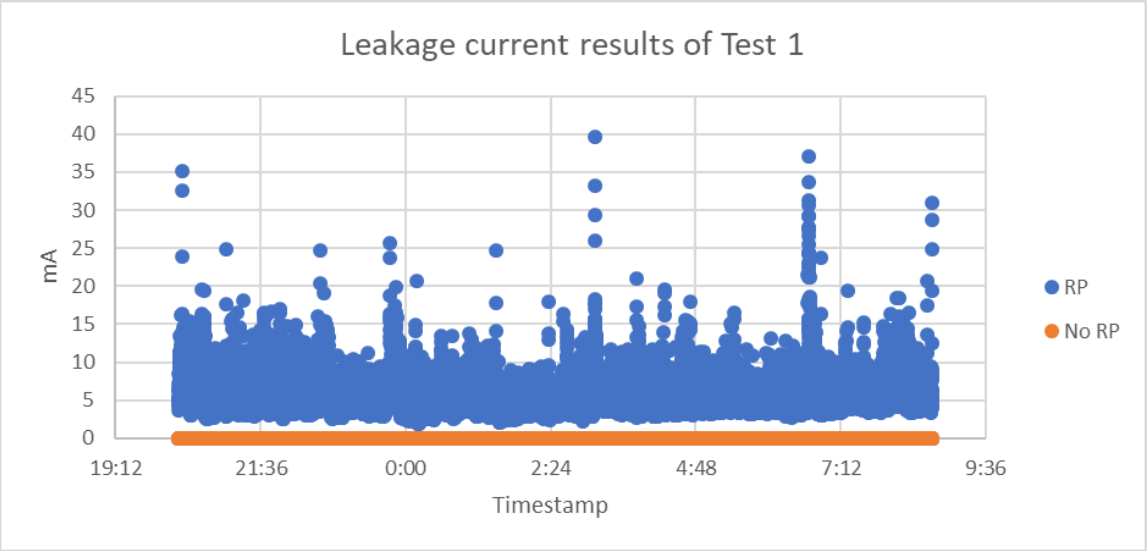


Figure 35. Leakage current results of Test 1.

Test 1 had been running for about 13h and at the end stopped with leakage current flowing through the red phosphorus containing DC plug's insulation reaching 100mA value. The current measured from the plug not containing red phosphorus is also presented on figure 35 and is virtually nonexistent.

Test 2 lasted for about 50min and was done to the same plugs involved in Test 1. Test 2 also stopped after the red phosphorus containing plug had reached 100mA leakage current. Below are the results of Test 2 (see figure 36):

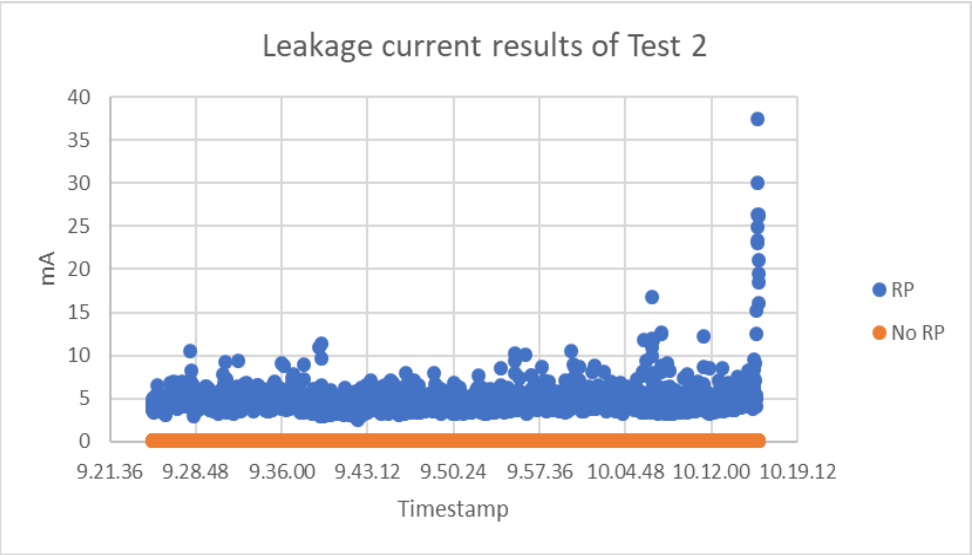


Figure 36. Leakage current results of Test 2.

Test 3 was done to a different plug and lasted only for about 11min to investigate initial current behavior. The test was stopped voluntarily. Results are presented on figure 37:

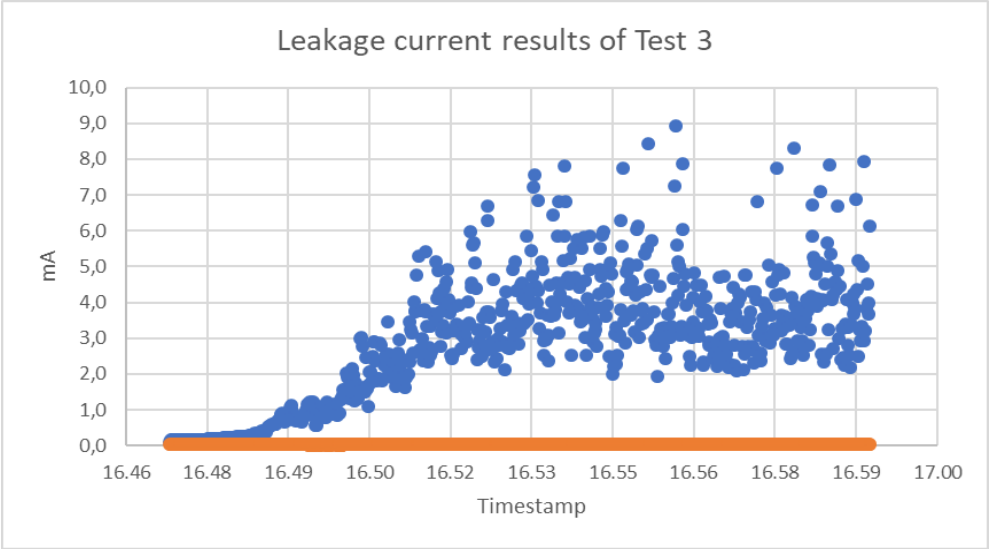


Figure 37. Leakage current results of Test 3.

Test 4 was conducted with a third plug containing red phosphorus and stopped after approximately 20min with the plug having leakage current of 100mA (see figure 38):

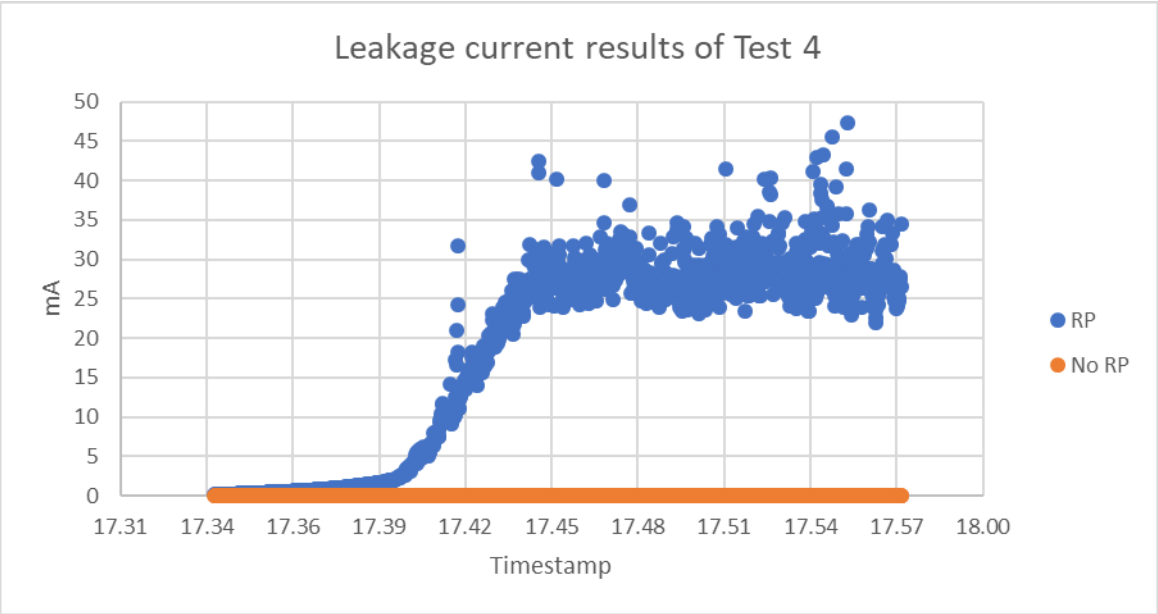


Figure 38. Leakage current results of Test 4.

Two out of three plugs tested accumulated green traces of corrosion on the inside of the plug (see figures 39 - 41):

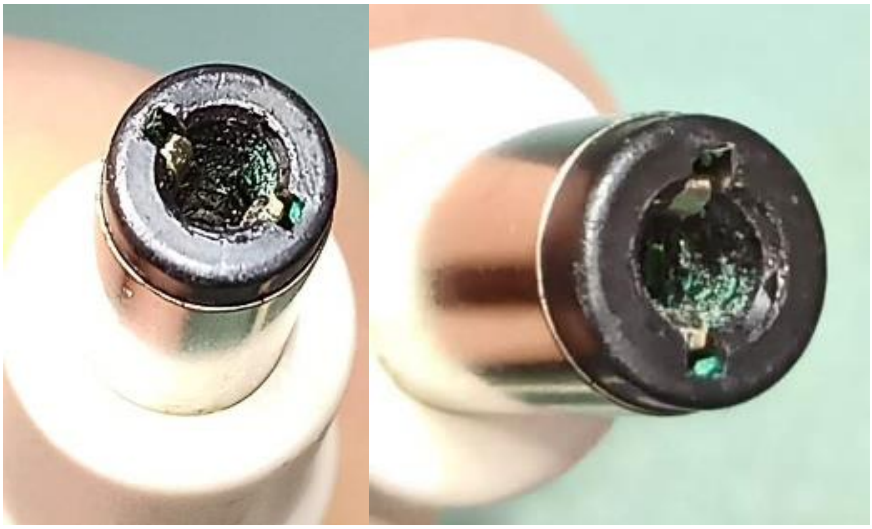

Figure 39. First plug under test. Green corrosion is apparent.

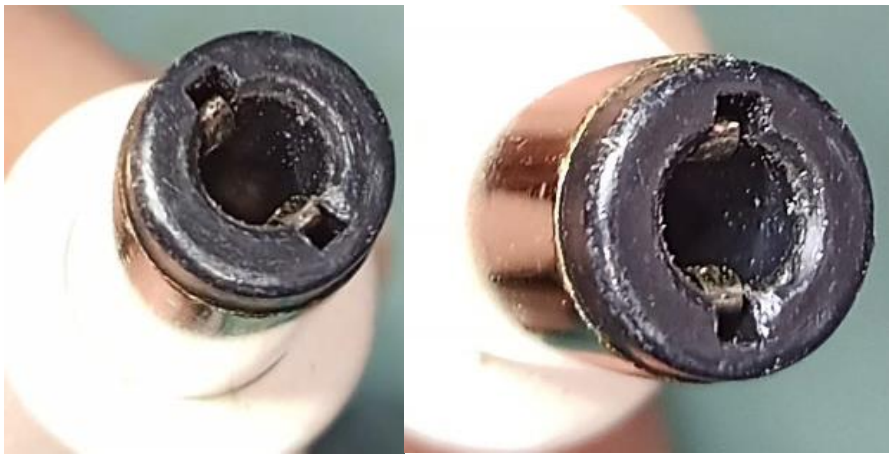

Figure 40. Clean plug that does not contain red phosphorus.

Figure 41. Second plug under test. Green corrosion is apparent.

The plug tested in the Test 4 did not accumulate visible traces of corrosion.

## 5 Discussion

The setup built for measurement is not claimed to be highly accurate. Results were compensated for the setup error measured in practice, yet the compensation procedure did not eliminate the measurement error completely, one reason being $|Iactual - Imeasured|$ used for evaluating errors instead of the actual $Iactual - Imeasured$ parameter.

The results presented clearly indicate that the leakage current observed in the red phosphorus plugs during the accelerated lifetime test exceeded the expected limits and that the insulation of the plug failed or, in case of Test 3, would have failed if the test had been continued. On the opposite, the leakage current of the plug that does not contain red phosphorus was negligibly small in all four tests.

Leakage current induced by the insulation failure in all four tests showed an intermittent behavior as it was expected based on the literature review, which indicates the presence of electrochemical migration processes leading to the development of current paths and then their subsequent destruction by a higher current.

In addition, the observation of corrosion traces developed on two out of three red phosphorus containing plugs partially align with the observations of copper corrosion pointed out in research paper by Chen *et al.* [8], where copper was corroded by red phosphorus and as a result copper phosphate was formed. The chemical composition of corrosion traces developed during the test would need to be studied separately to acquire further information.

Regarding the measurement setup, it has to be said that the measurement could have been simplified by a variety of means, first one being using Keithley 2000 Series multimeter connected straight to the plug and reporting the measured values via serial ports. Second optimization might have been to use differential ADC inputs of ATmega2560 to receive the differential output mode voltage directly, which could have eliminated the need for a precise voltage reference. An important comment is also that ADC accuracy specifications introduce significant amount of errors to the current measurement and using a 10-bit resolution ADC is generally not reasonable for low current measurements. In addition, one measurement PCB incorporating two current sense amplifiers could have been developed instead of the presented solution. Lastly, simulation tools obviously could have been used in order to anticipate and avoid design mistakes and their fixing in the prototyping stage of the design.

# 6 Conclusion

The target of the project presented herein was to conduct the reliability testing of red phosphorus containing DC plugs. In addition, possible behavior of insulation material failures in the form of conductive paths formation described in the literature was attempted to observe by a practical test. Though limited in accuracy and applicability for other current measurement needs, the setup built nevertheless served as a tool for registering insulation current changes and observing generalized trends of red phosphorus insulation failure behavior. During the experiment, red phosphorus containing DC plugs developed intermittent leakage currents, and therefore failed the reliability test. The target of the project is thus met.

To compliment the results of the experiment presented in this work and to acquire better understanding of insulation failures observed, investigations with, for example, Scanning electron microscopy (SEM) or Superconducting quantum interference device (SQUID) could have been conducted further to provide some valuable information on the physical and chemical nature of conductive paths developed. In addition, a third-party chemical investigation would have been needed to verify that the corrosion developed on the plug is of a phosphorus salt nature.

No generalized conclusion on the reliability of red phosphorus as a flame retardant in electronic applications can however be made as the exact red phosphorus manufacturing process used in the insulation of the plugs under test remains unknown to KaVo Kerr and cannot be investigated further. It is obvious, however, that red phosphorus containing insulation materials have to be carefully considered and tested prior to the planning on their use in a product with long life requirements. Such failures in the insulation might lead to the fire, if the current flowing through insulation is not limited by other protection means.

## References


1 Nishizawa H. Flame Retardant Agents. Journal of the Society of Rubber Industry, Japan 2006;79(6):316-322.

2 Ardebili H, Pecht MG. Encapsulation Technologies for Electronic Applications. Oxford, UK: William Andrew Applied Science Publishers; 2009.

3 Pecht M, Deng Y. Electronic device encapsulation using red phosphorus flame retardants. Microelectronics Reliability 2006;46;53-62.

4 Deng Y, Pecht M, Rogers K. Analysis of Phosphorus Flame Retardant Induced Leakage Currents in IC Packages Using SQUID Microscopy. IEEE Transactions on Components and Packaging Technologies 2006;29(4);804-808. URL: https://ieeexplore.ieee.org/abstract/document/4016216. Accessed 24 April 2020.

5 Hillman C. White Paper: Red Phosphorus Induced Failures in Encapsulated Circuits [online]. College Park, Maryland: DfR Solutions. URL: https://www.dfrsolutions.com/ red-phosphorus-induced-failures-in-encapsulated-circuits. Accessed 24 April 2020.

6 Somayajulu MR, Gautam GK, Subhananda Rao A. Stabilisation of Red Phosphorus to Prevent Moisture Absorption and Suppression of Phosphine Release. Defence Science Journal 2007;57(6);517-824. URL: http://citeseerx.ist.psu.edu/viewdoc/ download?doi=10.1.1.1008.6843&rep=rep1&type=pdf. Accessed 24 April 2020.

7 Wilson R. Solutions To Black Exercises For Chemistry: The Central Science. 11th ed. Upper Saddle River, NJ : Pearson Prentice Hall; 2009. URL: https://www.chegg.com/homework-help/ structures-white-red-phosphorus-shown-explain-using-structu-chapter-22-problem-9vc-solution-9780136003243-exc. Accessed 24 April 2020.

8 Chen Z, Du J, Li X, Xie Z, Wang Y, Wang H, Zheng J, Yang R. Failure behavior of nylon products for red phosphorus flame retardant electrical connectors. RSC Advances 2019;43(9);24935–24941.

9 Wang N, Wu J, Daniel S. Failure analysis of intermittent pin-to-pin short caused by phosphorous particle in molding compound. San Jose, CA: 2005 IEEE International Reliability Physics Symposium, 2005. Proceedings. 43rd Annual; 2005. p.580-581. URL: https://ieeexplore.ieee.org/abstract/document/1493152. Accessed 25 April 2020.

10 Hylton RR. Techniques for Identification of Silver Migration in Plastic Encapsulated Devices Assembled with Molding Compound Containing Red Phosphorus Flame Retardant Material. Portland, Oregon: ISFTA 2008: Proceedings from the 34th International Symposium for Testing and Failure Analysis; 2008. p.112-120.

11 Deng Y, Pecht M. The Story Behind the Red Phosphorus Mold Compound Device Failures. Tokyo, Japan: 2005 International Symposium on Electronics Materials and Packaging (EMAP2005); 2005. p.1-5.

12 Hillman C. Red Phosphorus Reliability Alert [online]. Beltsville, MD: DfR Solutions; 4 June 2015.
URL: https://www.dfrsolutions.com/resources/
product-reliability-alert-red-phosphorous. Accessed 25 April 2020.

13 Rin Kagaku Kogyo Co., Ltd. The features of red phosphorus flame retardants [online]. Toyama, Japan: Rin Kagaku Kogyo Co., Ltd.; March 2019.
URL: http://www.rinka.co.jp/english/products/flame-retardant/advantage.html. Accesssed 26 April 2020.

14 International Electrotechnical Commission. Working Draft of IEC 60601-1 Ed. 3.2 Medical electrical equipment – Part 1: General requirements for safety and essential performance. Geneva, Switzerland: IEC; 2018.

15 Zhan S, Azarian MH, Pecht M. Reliability of Printed Circuit Boards Processed Using No-Clean Flux Technology in Temperature–Humidity–Bias Conditions. IEEE Transactions on Device and Materials Reliability 2008;8(2);426-434.

16 Yarborough B. Components and Methods for Current Measurement [online]. Nashville, TN: Endeavor Business Media, LLC; 6 January 2012.
URL: https://www.powerelectronics.com/technologies/
power-electronics-systems/article/21861306/
components-and-methods-for-current-measurement. Accessed 26 April 2020.

17 Texas Instruments. Simplifying Current Sensing [online]. Dallas, Texas: Texas Instruments Incorporated; 2020.
URL: http://www.ti.com/lit/ml/slyy154a/slyy154a.pdf. Accessed 26 April 2020.

18 Hill S. External current sense amplifiers versus integrated onboard amplifiers for current sensing [online]. Dallas, Texas: Texas Instruments Incorporated; February 2019.
URL: https://www.digikey.com/short/zzp9f0. Accessed 26 April 2020.

19 Maxim Integrated. Tutorials 746: High-Side Current-Sense Measurement: Circuits And Principles [online]. San Jose, CA: Maxim Integrated Products, Inc; 19 November 2001.
URL: http://www.maximintegrated.com/an746. Accessed 26 April 2020.

20 Regan T, Munson J, Zimmer G, Stokowski M. Application Note 105: Current Sense Circuit Collection [online]. Milpitas, CA: Linear Technology Corporation; December 2005.
URL: https://www.analog.com/media/en/technical-documentation/
application-notes/an105fa.pdf. Accessed 26 April 2020.

21 Leibson S. Fundamentals of Current Measurement: Part 2 – Current Sense Amplifiers [online]. Thief River Falls, MN: Digi-Key's North American Editors; 7 November 2018.
URL: https://www.digikey.fi/en/articles/fundamentals-of-current-measurement-part-2-current-sense-amplifiers. Accessed 26 April 2020.

22 Riedel M, Schwarzbach M. Current measurement with auto-ranging yields 30dB range dynamics [online]. Berlin, Germany: imc Test & Measurement GmbH; 28 August 2018.
URL: https://www.imc-tm.com/fileadmin/Public/Downloads/Whitepapers/WP_EN/WP_eng_Current_Measurement_with_Auto-Ranging.pdf. Accessed 26 April 2020.

23 Pini A. Select and Apply Current Sense Amplifiers Effectively to Better Manage Power [online]. Thief River Falls, MN: Digi-Key's North American Editors; 21 August 2018.
URL: https://www.digikey.fi/en/articles/select-apply-current-sense-amplifiers-effectively-manage-power. Accessed 26 April 2020.

24 Tallada S. TI Designs: TIDA-03050 Automotive, mA-to-kA Range, Current Shunt Sensor Reference Design [online]. Dallas, Texas: Texas Instruments Incorporated; December 2017.
URL: http://www.ti.com/lit/ug/tidud33a/tidud33a.pdf. Accessed 26 April 2020.

25 Texas Instruments. PGA281 Precision, Zero-Drift, High-Voltage, Programmable Gain Instrumentation Amplifier [online]. Dallas, Texas: Texas Instruments Incorporated; June 2013.
URL: http://www.ti.com/lit/ds/symlink/pga281.pdf. Accessed 27 April 2020.

26 Williams I. TI Precision Designs: Verified Design 10 µA-100 mA, 0.05% Error, High-Side Current Sensing [online]. Dallas, Texas: Texas Instruments Incorporated; September 2013.
URL: http://www.ti.com/lit/ug/tidu033/tidu033.pdf. Accessed 27 April 2020.

27 Texas Instruments. PGA281EVM User's Guide [online]. Dallas, Texas: Texas Instruments Incorporated; May 2013.
URL: http://www.ti.com/lit/ug/sbou130/sbou130.pdf. Accessed 27 April 2020.

28 ON Semiconductor. KA431S / KA431SA / KA431SL Programmable Shunt Regulator [online]. Aurora, Colorado: Semiconductor Components Industries, LLC; March 2015.
URL: https://www.onsemi.com/pub/Collateral/KA431SL-D.pdf. Accessed 27 April 2020.

29 Vishay Semiconductors. BYV27-50, BYV27-100, BYV27-150, BYV27-200 Ultra-Fast Avalanche Sinterglass Diode [online]. Malvern, PA: Vishay Intertechnology, Inc; 4 September 2012.
URL: http://www.vishay.com/docs/86042/byv27.pdf. Accessed 27 April 2020.

30 Gammon N. ADC conversion on the Arduino (analogRead) [online]. Mountain View, CA: Creative Commons Attribution 3.0 Australia; 27 February 2015. URL: https://www.gammon.com.au/adc. Accessed 27 April 2020.

31 Atmel. ATmega640/V-1280/V-1281/V-2560/V-2561/V Datasheet [online]. San Jose, CA: Atmel Corporation; February 2014. URL: https://ww1.microchip.com/downloads/en/devicedoc/atmel-2549-8-bit-avr-microcontroller-atmega640-1280-1281-2560-2561_datasheet.pdf. Accessed 27 April 2020.

## PCB Schematics

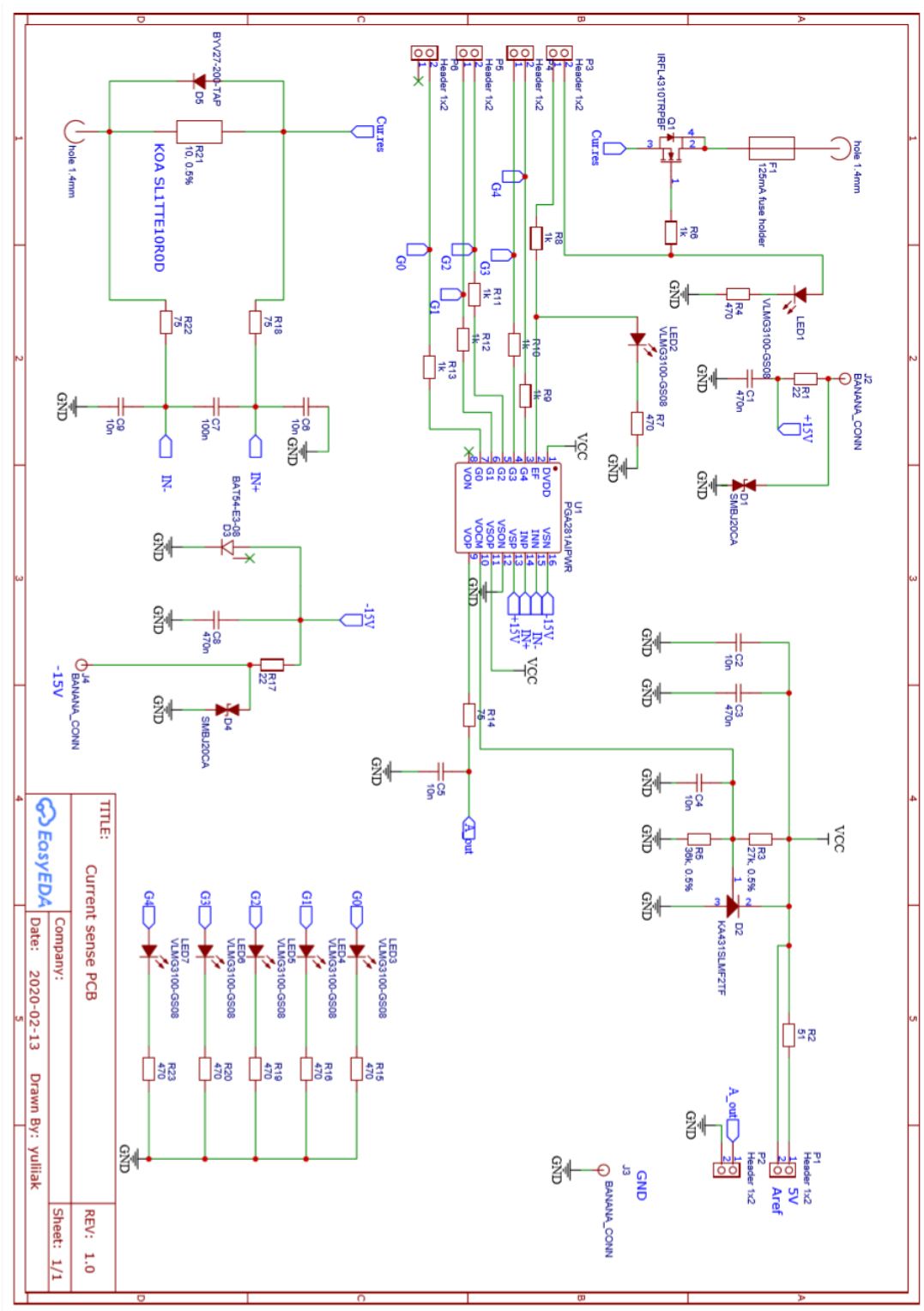

## PCB Layout

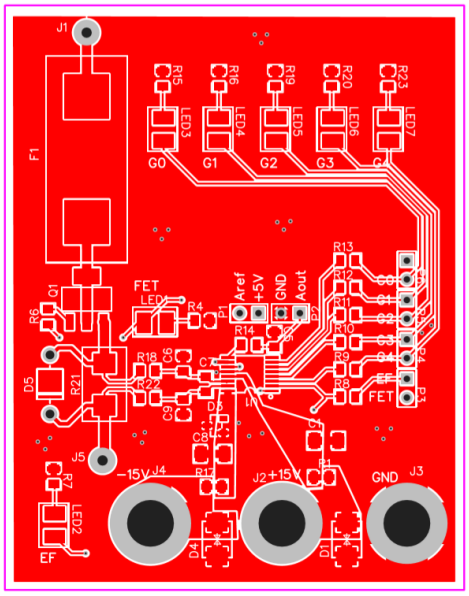


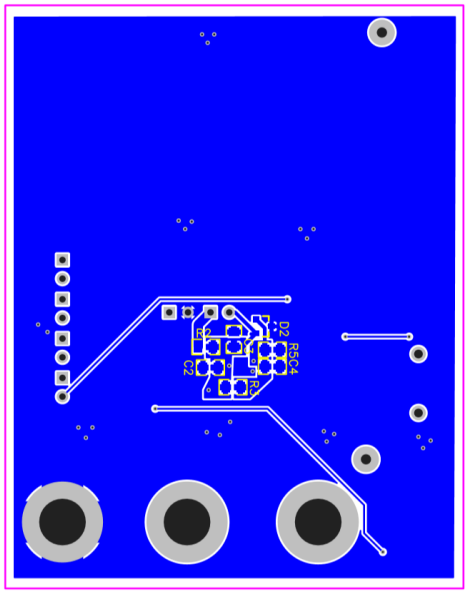

**TOP SIDE** **BOTTOM SIDE**

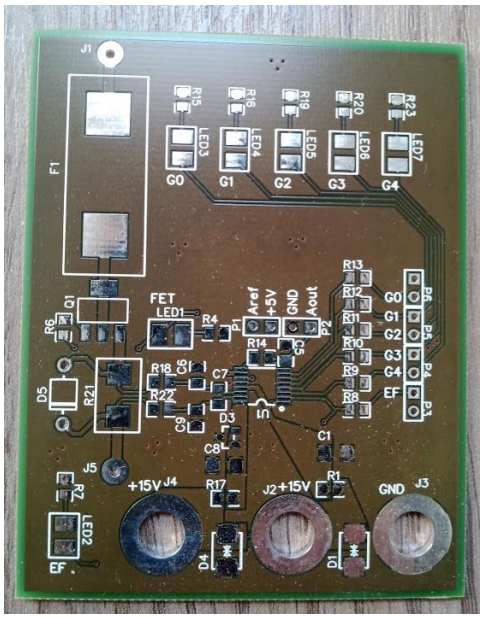


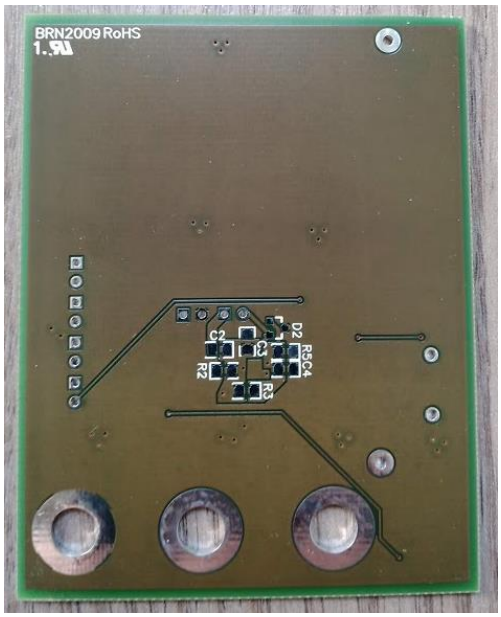


Some silkscreen errors discovered only after the board had been manufactured have been corrected on the layout picture.

## Arduino Code

```
//Definition of used digital pins for gain setting
int G1[]={49,50,51,52,53};
int G2[]={22,23,24,25,26};
int Stop_pin1=46;
int Stop_pin2=30;
//Definition for the variables that are stored as history of measurement for
running average.
const int numReadings = 10;
int readings1[numReadings],readings2[numReadings];
//gains taken from the datasheet, defined as bool arrays
bool uGain[]={0,1,0,1,1};//176
bool mGain[]={1,0,1,0,1};//5.5
bool Gain1[5], Gain2[5];
float numGain1=176, numGain2=176;
int i, n=0, prev_overload1 = 0, prev_overload2 = 0, overload_count1 = 0,
overload_count2 = 0, sensorValue1, sensorValue2;
unsigned long currtime=0;
float measured_current1, measured_current2, meas_min_current1,
meas_min_current2, meas_max_current1, meas_max_current2, meas_min1, meas_min2,
meas_max1, meas_max2, meas_v1, meas_v2, meas_max_v1, meas_max_v2, meas_min_v1,
meas_min_v2, adc_gain1 =0, adc_gain2=0, running_avg1 = 0, running_avg2=0,
average1 = 0, average2 = 0, d_adc_gain1=0, d_adc_gain2 = 0;
float k1=4.2186749e-14, k2=6.3283404e-11, k3=3.5311270e-8, k4=8.8979011e-6,
k5=9.6175701e-4, k6=6.9201321e-2;

void setup() {
Serial.begin(9600);
while(!Serial)
{}
//Used external analog reference of 4.453V
analogReference(EXTERNAL);
//definition of digital inputs
for (i=0;i<5;i++)
{pinMode(G1[i], OUTPUT);
pinMode(G2[i],OUTPUT);}
pinMode(Stop_pin1,OUTPUT);
pinMode(Stop_pin2,OUTPUT);
//intially expected that current is in uA range.
for (i=0;i<5;i++)
  {
  Gain1[i] = uGain[i];
  Gain2[i] = uGain[i];
  }
memset(readings1,0,sizeof(readings1));
memset(readings2,0,sizeof(readings2));
//FETs are ON.
digitalWrite(Stop_pin1,1);
digitalWrite(Stop_pin2,1);
}

void loop() {
//the loop lasts appr a second
currtime=millis();
n=0;
adc_gain1=0;
adc_gain2=0;
average1=0;
```

```
average2=0;
measured_current1=0;
measured_current2=0;
meas_min1=1024;
meas_min2=1024;
meas_max1=0;
meas_max2=0;
while (millis()<currtime+1000)
  {
  running_avg1=0;
  running_avg2=0;
//setting the gain to 176
  for (i=0;i<5;i++)
    {
    digitalWrite(G1[i], Gain1[i]);
    digitalWrite(G2[i], Gain2[i]);
    }
  sensorValue1 = analogRead(A0);
  sensorValue2 = analogRead(A1);
  readings1[n%numReadings]=sensorValue1;
  readings2[n%numReadings]=sensorValue2;
//running average calculation
  for (i=0;i<numReadings;i++)
    {
    running_avg1 +=readings1[i];
    running_avg2 +=readings2[i];
    }
  running_avg1 = running_avg1/numReadings;
  running_avg2 = running_avg2/numReadings;
  n++;
//calculation of (ADC- ADC offset)/gain
  d_adc_gain1 = (sensorValue1-577)/numGain1;
  d_adc_gain2 = (sensorValue2-577)/numGain2;
  adc_gain1 += d_adc_gain1;
  adc_gain2 += d_adc_gain2;
  meas_min1=min(d_adc_gain1,meas_min1);
  meas_min2=min(d_adc_gain2,meas_min2);
  meas_max1=max(d_adc_gain1,meas_max1);
  meas_max2=max(d_adc_gain2,meas_max2);
  if (((numGain1 == 176) && (sensorValue1 >= 993))&&((running_avg1 >=
993)&&(sensorValue1 >= running_avg1)))
    {
    Serial.println("SWITCHED TO 5.5");
    numGain1 = 5.5;
    for (i=0;i<5;i++)
      {
      Gain1[i]=mGain[i];
      }
    overload_count1=0;
    delay(100);
    }

  if (((numGain2 == 176) && (sensorValue2 >= 993))&&((running_avg2 >=
993)&&(sensorValue2 >= running_avg2)))
    {
    Serial.println("SWITCHED TO 5.5");
    numGain2 = 5.5;
    for (i=0;i<5;i++)
      {
      Gain2[i]=mGain[i];
      }
    overload_count2=0;
```

```
    delay(100);
    }
//stop the test by putting FET OFF if current is more than 100mA for 10 meas-
urements in a row.
  if ((overload_count1 == 10)|| (overload_count2 == 10))
    {
    while(true)
      {
      if (overload_count1 == 10)
      {digitalWrite(Stop_pin1,0);}
      if (overload_count2 == 10)
      {digitalWrite(Stop_pin2,0);}
      Serial.println("STOP");
      delay(1000);
      }
    }
  if (((numGain1 == 5.5)&&(sensorValue1 <= 580))&&((running_avg1 <=
580)&&(sensorValue1 <= running_avg1)))
    {
    Serial.println("SWITCHED TO 176");
    numGain1=176;
    for (i=0;i<5;i++)
      {
      Gain1[i]=uGain[i];
      }
    overload_count1=0;
    }
  else if ((numGain1==5.5)&&(sensorValue1 >=965))
    {
    overload_count1++;
    }
  else
    {
    overload_count1=0;
    }

  if (((numGain2 == 5.5)&&(sensorValue2 <= 580))&&((running_avg2 <=
580)&&(sensorValue2 <= running_avg2)))
    {
    Serial.println("SWITCHED TO 176");
    numGain2=176;
    for (i=0;i<5;i++)
      {
      Gain2[i]=uGain[i];
      }
    overload_count2=0;
    }
  else if ((numGain2==5.5)&&(sensorValue2 >=965))
    {
    overload_count2++;
    }
  else
    {
    overload_count2=0;
    }
  }
//after the second, compute the average.

average1=adc_gain1/n;
average2=adc_gain2/n;
//multiply the average by 1LSB*2
meas_v1 = average1*4.328125*2;
```

```
meas_v2 = average2*4.328125*2;
//8 digit precision coefficients used
measured_current1 = k1*pow(meas_v1,6)-k2*pow(meas_v1,5)+k3*pow(meas_v1,4)-
k4*pow(meas_v1,3)+k5*pow(meas_v1,2)+k6*meas_v1;
measured_current2 = k1*pow(meas_v2,6)-k2*pow(meas_v2,5)+k3*pow(meas_v2,4)-
k4*pow(meas_v2,3)+k5*pow(meas_v2,2)+k6*meas_v2;
meas_min_v1 = meas_min1*4.328125*2;
meas_min_v2 = meas_min2*4.328125*2;
meas_min_current1 = k1*pow(meas_min_v1,6)-
k2*pow(meas_min_v1,5)+k3*pow(meas_min_v1,4)-
k4*pow(meas_min_v1,3)+k5*pow(meas_min_v1,2)+k6*meas_min_v1;
meas_min_current2 = k1*pow(meas_min_v2,6)-
k2*pow(meas_min_v2,5)+k3*pow(meas_min_v2,4)-
k4*pow(meas_min_v2,3)+k5*pow(meas_min_v2,2)+k6*meas_min_v2;
meas_max_v1 = meas_max1*4.328125*2;
meas_max_v2 = meas_max2*4.328125*2;
meas_max_current1 = k1*pow(meas_max_v1,6)-
k2*pow(meas_max_v1,5)+k3*pow(meas_max_v1,4)-
k4*pow(meas_max_v1,3)+k5*pow(meas_max_v1,2)+k6*meas_max_v1;
meas_max_current2 = k1*pow(meas_max_v2,6)-
k2*pow(meas_max_v2,5)+k3*pow(meas_max_v2,4)-
k4*pow(meas_max_v2,3)+k5*pow(meas_max_v2,2)+k6*meas_max_v2;
Serial.print(measured_current1,10);
Serial.print('\t');
Serial.print(meas_max_current1,10);
Serial.print('\t');
Serial.print(meas_min_current1,10);
Serial.print('\t');
Serial.print(measured_current2,10);
Serial.print('\t');
Serial.print(meas_max_current2,10);
Serial.print('\t');
Serial.print(meas_min_current2,10);
Serial.println();
}
```

## TeraTerm .txt File Creation Script

```
filecreate file 'test.txt'
result=1

while result=1
  ; receive one line
  recvln
  ; write it to the log file
gettime timestr
filewrite file timestr
filewrite file ''#9

  filewriteln file inputstr
endwhile

fileclose file
closett
end
```

## Final Verification Data

*uA range current measurement:*

| I measured, mA | I actual, mA | \|delta\|,mA | error, % |
|---|---|---|---|
| 0,028 | 0,05 | 0,022 | 44 |
| 0,035 | 0,06 | 0,025 | 41,66667 |
| 0,043 | 0,07 | 0,027 | 38,57143 |
| 0,049 | 0,08 | 0,031 | 38,75 |
| 0,056 | 0,09 | 0,034 | 37,77778 |
| 0,063 | 0,1 | 0,037 | 37 |
| 0,07 | 0,11 | 0,04 | 36,36364 |
| 0,1 | 0,151 | 0,051 | 33,77483 |
| 0,135 | 0,2 | 0,065 | 32,5 |
| 0,172 | 0,251 | 0,079 | 31,4741 |
| 0,21 | 0,301 | 0,091 | 30,23256 |
| 0,225 | 0,321 | 0,096 | 29,90654 |
| 0,257 | 0,361 | 0,104 | 28,80886 |
| 0,306 | 0,426 | 0,12 | 28,16901 |
| 0,403 | 0,552 | 0,149 | 26,99275 |
| 0,43 | 0,587 | 0,157 | 26,74617 |
| 0,544 | 0,73 | 0,186 | 25,47945 |
| 0,634 | 0,838 | 0,204 | 24,34368 |
| 0,696 | 0,912 | 0,216 | 23,68421 |
| 0,723 | 0,943 | 0,22 | 23,3298 |
| 0,791 | 1,024 | 0,233 | 22,75391 |
| 0,804 | 1,039 | 0,235 | 22,6179 |
| 0,841 | 1,085 | 0,244 | 22,48848 |
| 0,881 | 1,128 | 0,247 | 21,89716 |
| 0,894 | 1,142 | 0,248 | 21,71629 |
| 0,905 | 1,155 | 0,25 | 21,64502 |
| 0,987 | 1,246 | 0,259 | 20,78652 |
| 1,057 | 1,327 | 0,27 | 20,34665 |
| 1,134 | 1,411 | 0,277 | 19,63147 |
| 1,153 | 1,432 | 0,279 | 19,48324 |
| 1,191 | 1,473 | 0,282 | 19,1446 |
| 1,205 | 1,49 | 0,285 | 19,12752 |
| 1,237 | 1,526 | 0,289 | 18,9384 |
| 1,383 | 1,682 | 0,299 | 17,77646 |
| 1,41 | 1,711 | 0,301 | 17,59205 |
| 1,533 | 1,84 | 0,307 | 16,68478 |
| 1,616 | 1,923 | 0,307 | 15,96464 |

*mA current measurement range:*

| I measured, mA | I actual, mA | \|delta\|, mA | error, % |
|---|---|---|---|
| 0,483 | 0,94 | 0,457 | 48,61702 |
| 0,756 | 1,272 | 0,516 | 40,56604 |
| 1,78 | 2,371 | 0,591 | 24,92619 |
| 3,233 | 3,766 | 0,533 | 14,15295 |
| 4,802 | 5,167 | 0,365 | 7,06406 |
| 6,991 | 7,062 | 0,071 | 1,005381 |
| 9,211 | 9,032 | 0,179 | 1,981842 |
| 10,422 | 10,127 | 0,295 | 2,913005 |
| 13,215 | 12,862 | 0,353 | 2,744519 |
| 15,545 | 15,304 | 0,241 | 1,574752 |
| 17,175 | 17,061 | 0,114 | 0,668191 |
| 18,93 | 19,01 | 0,08 | 0,420831 |
| 20,132 | 20,36 | 0,228 | 1,119843 |
| 22,646 | 23,057 | 0,411 | 1,782539 |
| 24,49 | 24,952 | 0,462 | 1,851555 |
| 26,672 | 27,118 | 0,446 | 1,644664 |
| 28,729 | 29,048 | 0,319 | 1,098182 |
| 29,882 | 30,114 | 0,232 | 0,770406 |
| 32,034 | 32,088 | 0,054 | 0,168287 |
| 33,518 | 33,433 | 0,085 | 0,25424 |
| 35,34 | 35,081 | 0,259 | 0,738291 |
| 37,412 | 37,011 | 0,401 | 1,083462 |
| 40,732 | 40,265 | 0,467 | 1,159816 |
| 43,296 | 42,999 | 0,297 | 0,690714 |
| 45,125 | 45,06 | 0,065 | 0,144252 |
| 47,041 | 47,276 | 0,235 | 0,497081 |
| 48,469 | 48,927 | 0,458 | 0,936088 |
| 49,51 | 50,094 | 0,584 | 1,165808 |
| 52,183 | 53,031 | 0,848 | 1,599065 |
| 54,036 | 55,013 | 0,977 | 1,775944 |
| 56,122 | 57,249 | 1,127 | 1,968593 |
| 57,463 | 58,72 | 1,257 | 2,140668 |
| 55,982 | 57,062 | 1,08 | 1,892678 |
| 58,87 | 60,167 | 1,297 | 2,155667 |
| 59,739 | 61,187 | 1,448 | 2,366516 |
| 60,781 | 62,35 | 1,569 | 2,516439 |
| 63,295 | 65,052 | 1,757 | 2,700916 |
| 64,939 | 66,93 | 1,991 | 2,97475 |
| 67,862 | 70,157 | 2,295 | 3,271235 |
| 71,956 | 75,221 | 3,265 | 4,340543 |
| 74,528 | 78,254 | 3,726 | 4,761418 |
| 80,14 | 85,357 | 5,217 | 6,111977 |
| 81,951 | 87,349 | 5,398 | 6,179807 |
| 84,713 | 90,273 | 5,56 | 6,159095 |
| 87,978 | 95,15 | 7,172 | 7,537572 |
| 92,185 | 100,086 | 7,901 | 7,894211 |